ASTROBIOLOGY
Volume 23, Number 9, 2023

DOI: 10.1089/ast.2022.0137

Effects of UV and Calcium Perchlorates on Uracil Deposited on Strontium Fluoride Substrates at Mars Pressure and Temperature

N. Chaouche-Mechidal,[1] F. Stalport,[2] E. Caupos,[1,3] E. Mebold,[4] C. Azémard,[1] C. Szopa,[5] P. Coll,[2] and H. Cottin[1]

Abstract

Organic matter is actively searched on Mars with current and future space missions as it is a key to detecting potential biosignatures. Given the current harsh environmental conditions at the surface of Mars, many organic compounds might not be preserved over a long period as they are exposed to energetic radiation such as ultraviolet light, which is not filtered above 190 nm by the martian atmosphere. Moreover, the presence of strong oxidizing species in the regolith, such as perchlorate salts, might enhance the photodegradation of organic compounds of astrobiological interest. Because current space instruments analyze samples collected in the upper surface layer, it is necessary to investigate the stability of organic matter at the surface of Mars. Previous experimental studies have shown that uracil, a molecule relevant to astrobiology, is quickly photolyzed when exposed to UV radiation under the temperature and pressure conditions of the martian surface with an experimental quantum efficiency of photodecomposition (φ_{exp}) of 0.30 ± 0.26 molecule$\cdot$photon^{-1}. Moreover, the photolysis of uracil leads to the formation of more stable photoproducts that were identified as uracil dimers. The present work aims to characterize the additional effect of calcium perchlorate detected on Mars on the degradation of uracil. Results show that the presence of calcium perchlorate enhances the photodecomposition of uracil with $\varphi_{exp} = 12.3 \pm 8.3$ molecule$\cdot$photon^{-1}. Although some of the photoproducts formed during these experiments are common to those formed from pure uracil only, the Fourier transformation infrared (FTIR) detection of previously unseen chemical functions such as alkyne C ≡ C or nitrile C ≡ N has shown that additional chemical species are formed in the presence of calcium perchlorate in the irradiated sample. This implies that the effect of calcium perchlorate on the photolysis of uracil is not only kinetic but also related to the nature of the photoproducts formed. Key Words: Mars—Organic matter—UV irradiation—Calcium perchlorate—Nucleobases—Pyrimidine. Astrobiology 23, 959–978.

1. Introduction

1.1. Organic matter on Mars

During their early history, Mars and Earth were similar as they both presented conditions thought to be favorable for the emergence of life such as liquid water. Due to extensive geomorphological (*e.g.,* valley networks) and mineralogical (*e.g.,* phyllosilicates) evidence of past stable water (Poulet *et al.,* 2005; Mustard *et al.,* 2008; Ehlmann *et al.,* 2013), the search for past and/or present life on Mars has become a major goal for the exploration of Mars. Because life on Earth is based on organic matter, the detection of organic molecules that might originate from biotic sources could be a hint of possible prebiotic chemistry or ancient life

[1]Univ Paris Est Creteil and Université Paris Cité, CNRS, LISA, F-94010 Créteil, France.
[2]Université Paris Cité and Univ Paris Est Creteil, CNRS, LISA, F-75013 Paris, France.
[3]Ecole des Ponts, LEESU, F-77455 Champs-sur-Marne, France.
[4]Univ Paris Est Creteil, CNRS, OSU-EFLUVE, F-94010 Créteil, France.
[5]LATMOS/IPSL, UVSQ Université Paris-Saclay, Sorbonne Université, CNRS, 78280 Guyancourt, France.

on early Mars. Therefore, the search for organic matter on Mars is one of the major goals of current and future space missions such as Mars Science Laboratory (MSL) (Grotzinger *et al.,* 2012), Mars 2020 (Farley *et al.,* 2020), and ExoMars (Vago *et al.,* 2017). However, for a better interpretation of the data collected by *in situ* instruments, it is necessary to consider that organic matter on Mars might also have originated from abiotic sources.

To date, the only verified source of organic matter is exogenous to Mars. Like Earth, Mars is subject to bombardments of meteorites with an annual delivery of organic matter estimated to be 10^6 kg (Flynn, 1996). Some of these meteorites are referred to as carbonaceous chondrites and are of high carbon content ($\sim$3.5% wt) (Alexander *et al.,* 2017). Chemical analyses of terrestrial chondrite meteorites have been well documented and show the presence of various organic molecular species. A major part of the organic carbon content (at least 70%) is qualified as insoluble organic matter (IOM) and represents macromolecular structures involving mainly aromatic hydrocarbons (Alexander *et al.,* 2017). The other part of the carbon content (less than 30%) is solvent-soluble organic molecules and includes various prebiotic organic species (amino acids, nucleobases, carboxylic acids…) (Sephton, 2002; Pizzarello *et al.,* 2006; Schmitt-Kopplin *et al.,* 2010; Oba *et al.,* 2022). As Mars still experiences meteorite bombardment, this meteoritic organic matter should reach to the surface. Therefore, a wide diversity of organic molecules is expected to be brought to Mars by the meteoritic influx particularly.

First detections of organic molecules on Mars have been performed by the Sample Analysis at Mars (SAM) instrument on board the Curiosity rover (MSL, 2012) on samples collected from the surface. *In situ* analysis of martian samples is carried out by using pyrolysis/derivatization coupled to gas chromatography and mass spectrometry (GC-MS) experiments (Mahaffy *et al.,* 2012). The origin of several chlorinated organic compounds has been attributed to organic matter endogenous to Mars that reacted with oxychlorines present in the samples (Freissinet *et al.,* 2015; Szopa *et al.,* 2020). However, it cannot be excluded that a fraction of these chlorine-bearing molecules is present in the soil. Additionally, Eigenbrode *et al.* (2018) reported diverse sulfur-bearing organic compounds such as thiophenes, which are detected when samples are submitted to the highest pyrolytic temperatures used by SAM (>600°C), potentially highlighting a second organic phase in the same samples producing chlorine-bearing species. More recently, wet chemistry experiments (derivatization) conducted with SAM revealed the detection of benzoic acid and ammonia in martian samples. Phosphoric acid, phenol, and several nitrogen-bearing molecules are also likely to be present in the samples (Millan *et al.,* 2021). Finally, the detection of methane is still debated but remains a possible source of organic matter in Mars' atmosphere (Knutsen *et al.,* 2021). Although organic matter was firmly detected at the surface of Mars, it is hard to associate the detected organic compounds to any possible source. Indeed, the detected molecules are quite different from those brought to Mars by exogenous sources.

Current problematics related to the detection of organic molecules is to understand those mechanisms that lead to differences observed between the actual detections and the sources of organic matter on Mars. Besides possible experimental biases, the impact of the martian environment on the preservation of organic molecules is the main hypothesis to explain these differences.

1.2. Impact of Mars' environment

Although Mars may have been habitable in the past, the current environmental conditions at the surface are not favorable to the preservation of simple prebiotic organic compounds (amino and carboxylic acids, nucleobases…) found in meteorites. Two main factors are likely to alter the organic matter on Mars (Svensson *et al.,* 1999): energetic radiation at the surface and subsurface, and/or oxidizing species in the regolith.

Because the magnetic field of Mars declined early in the planet's history, the atmosphere and surface became vulnerable to energetic radiation and particles such as galactic cosmic rays and solar energetic particles (Dartnell *et al.,* 2007; McKenna-Lawlor *et al.,* 2012; Ehresmann *et al.,* 2014; Matthia *et al.,* 2017). Among all the solar energetic radiation present on Mars, the surface is not protected from UV light. Unlike Earth, the current atmosphere of Mars does not filter UV light in the 190–400 nm range. Therefore, UV photons reach the surface and interact with the first millimeters of the regolith, which might initiate photochemical reactions (Patel *et al.,* 2002). The only *in situ* measurements of the UV flux reaching the surface of Mars were done by the REMS/UV sensor on board the Curiosity rover (MSL mission, 2012) in the 315–380 nm wavelength range (Martinez *et al.,* 2017). The generated data sets are corrected from dust deposition bias on the UV sensor (UVS). The total UV (A, B, C) flux measured between 200 and 380 nm by the Rover Environmental Monitoring Station (REMS) sensor on board the Curiosity rover represents 21 $W \cdot m^{-2}$ (Vicente-Retortillo *et al.,* 2020). To date, these corrected data are the most representative of the current UV flux on Mars in this spectral range and are important for UV laboratory experiments designed to extrapolate results with regard to the Mars case. Depending on the latitude, the season, and the atmospheric opacity, the total irradiance could vary from 2 to 55 $W \cdot m^{-2}$ at noon. The effect of direct exposure of organic molecules to UV light has been largely studied in the laboratory and in low Earth orbit experiments to explain the lack of diversity of organic molecules detected with regard to top surface sampling (Cottin, 2012; Fornaro *et al.,* 2013, 2018; Poch *et al.,* 2014; Carrier *et al.,* 2019; Stalport *et al.,* 2019).

On Mars, the identified oxidizing species suspected to degrade organic matter is perchlorate salts. These salts are presumed to be formed from UV-driven (or electrochemically driven) oxidation of Cl-bearing minerals on SiO_2 surfaces (Schuttlefield *et al.,* 2011; Carrier and Kounaves, 2015; Carrier, 2017; Wu *et al.,* 2018). First detections of perchlorate ions (ClO_4^-) were performed by the Phoenix lander with an abundance of 0.4–0.6% wt near the North Pole in Vastitas Borealis (Hecht *et al.,* 2009). The data show that the ClO_4^- parent salts were associated with Ca^{2+} and Mg^{2+} cations as a 60/40 mixture of $Ca(ClO_4)_2$ and $Mg(ClO_4)_2$ (Kounaves *et al.,* 2014b). Later, evidence of calcium perchlorate was interpreted from the analysis of martian sample regolith performed by SAM on Gale Crater

near the equator (Glavin *et al.,* 2013; Clark *et al.,* 2021). Moreover, the reanalysis of Viking lander mission data has corroborated the presence of perchlorates and chlorinated organic compounds at midlatitudes of Mars (Navarro-González *et al.,* 2010). Finally, chlorates and perchlorate salts were also identified in the EETA79001 and Tissint martian meteorites (Kounaves *et al.,* 2014a; Jaramillo *et al.,* 2019). As perchlorates have been detected in different regions of Mars and in martian meteorites, this gives good reasons for considering their distribution to be global. The detection of perchlorates on Mars is interesting as they could be a source of chlorine for the chlorinated compounds detected by SAM. Interestingly, a recent experimental study showed that perchlorates can be activated by UV light that decomposes ClO_4^- ions to ClO_3^- ions (chlorates) and other chlorine oxides species (Cl_yO_x). The UV-activated perchlorates enhanced the oxidation of methane to CO_2 and CO in the gas phase (Zhang *et al.,* 2022). These results suggest that the presence of perchlorate minerals in the presence of organic matter on Mars, when exposed to UV light, might also degrade organic molecules of interest for space missions. For the present study, we chose to work with calcium perchlorate as it has clearly been identified by two landing missions (Phoenix and MSL).

Laboratory simulation experiment is a useful tool with which to study the effects of the martian surface conditions on organic molecules of interest. It is also key to constraining the list of molecules that may be detected by *in situ* instruments. This work aims to explore the simultaneous effect of UV light and the presence of perchlorates on the behavior of organic molecules of interest on Mars.

1.3. The search for nucleobases on Mars

In this study, the targeted molecule is the pyrimidine uracil, which was selected due to the following three criteria: uracil is thought to be brought to Mars by exogenous sources (see below), is a prebiotic-relevant molecule, and is suspected to be resistant to alteration under martian conditions.

Nucleobases are fundamental coding components of the genetic macromolecules DNA and RNA in biological living cells. Their acid-base and mesomeric chemical properties make them chemically and photochemically active components (and therefore subject to evolve in the martian environment). These molecules have been detected in meteorites with a higher abundance of purines than pyrimidines (Callahan *et al.,* 2011). More recently, a wider variety of nucleobases have been detected in three carbonaceous meteorites (Murchison, Murray, and Tagish Lake) including various pyrimidines such as uracil (~1–15 ppb), thymine (~1–5 ppb), and cytosine (~2–5 ppb) (Oba *et al.,* 2022). Moreover, previous experiments have shown that irradiated pyrimidine in H_2O and/or NH_3 ices abiotically produces substituted nucleobases including these same pyrimidines (Materese *et al.,* 2013; Bera *et al.,* 2016). This implies that

Table 1. Molecular Structures of Uracil and Its Dimers as Deduced from Experimental Masses During Pure Uracil Irradiation Experiments

Molecule	Uracil	Uracil dimer	Uracil dimer
Molecular formula	$C_4H_4N_2O_2$	$C_8H_8N_4O_4$	$C_8H_6N_4O_3$
[M+H]+ theoretical *m/z* (amu)	113.034554	225.061832	207.051267
Chemical structure	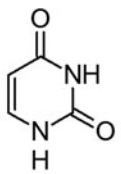	1' 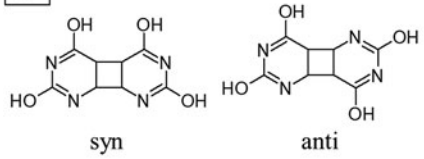 syn anti 2' 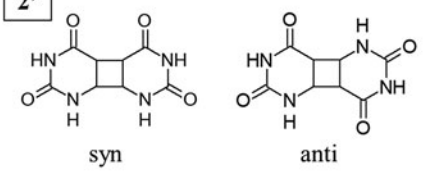 syn anti	3' 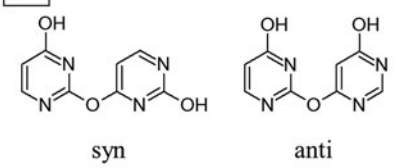 syn anti 4' 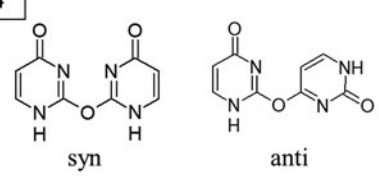 syn anti

Adapted from Rouquette *et al.* (2020).

these prebiotic-relevant compounds can be formed in space conditions (*e.g.,* chondrites) and could, therefore, be brought to the surface of rocky planets such as Earth and Mars.

Furthermore, previous studies have shown that irradiated pyrimidine nucleobases such as thymine can dimerize under UV light (Anderson *et al.,* 2019). Also, uracil (Table 1) has been studied specifically in Mars-like UV conditions (Rouquette *et al.,* 2020). The analysis of the UV-exposed sample by UHPLC-HRMS (ultra-high-performance liquid chromatography coupled with high-resolution mass spectrometry) showed that uracil produces Ura-Ura dimers under Mars-like UV light, temperature, and pressure conditions (Table 1). These dimers were more UV-resistant than uracil itself during the whole time of exposure (45 terrestrial days in the experiment). All these reasons make the uracil molecule a good candidate for the study of its chemical degradation in Mars-like surface conditions. In this study, we investigated the effect of calcium perchlorate on the degradation of uracil under Mars-like UV radiation conditions.

2. Methods

2.1. Sample preparation

The samples studied were prepared on a strontium fluoride (SrF_2) window. SrF_2 has interesting transmission properties (more than 90%) in the infrared (4000–950 cm^1) and ultraviolet (200-400 nm) spectral ranges. The sample is made up of a thin film of uracil and/or calcium perchlorate that is deposited on the SrF_2 window following one of these three procedures:

- Calcium perchlorate sample preparation:
  Tetra-hydrate calcium perchlorate ($Ca(ClO_4)_2 \cdot 4H_2O$) powder (Sigma-Aldrich, 99% purity) is diluted in water with a 0.5 $g \cdot L^{-1}$ concentration. A total of 100 µL of this solution was deposited on a SrF_2 window. Water is then evaporated at 100°C, and the sample is stored in a drying oven at 70°C until its use in the simulation experiment. The calcium perchlorate deposit is inspected visually first to ensure that the deposit has been correctly made and seems homogeneous. Deposits are analyzed by infrared spectroscopy at different locations in the sample simply by rotating the sample to see whether calcium perchlorates are present all over the deposit. It cannot be guaranteed that the thickness of the deposit is homogeneous, but our infrared analysis will average results over surfaces with scales larger than noticeable inhomogeneities of the deposit.
- Uracil sample preparation:
  Uracil ($C_4H_4N_2O_2$) (Sigma-Aldrich, ≥99% purity) is deposited as a thin (200–400 nm thickness) and homogeneous organic layer. The organic deposit is obtained by sublimation of the organic powder (see details in Guan *et al.,* 2010). Organic molecules are heated at their sublimation temperature (130°C) in an oven placed in a vacuum chamber (10^{-5} mbar). Sublimated organic molecules condensate on the SrF_2 windows above the oven. Uracil deposit samples are then stored in the dark at ambient temperature and pressure. In the context of this study, these uracil samples were used as references to highlight any effect of calcium perchlorate during sample preparation.
- Uracil and calcium perchlorate sample preparation:
  Samples containing a tetra-hydrate perchlorate ($Ca(ClO_4)_2 \cdot 4H_2O$) and a film of uracil are obtained by combining both methods cited above. This technique leads to a bilayer sample with a calcium perchlorate deposit covered by a film of uracil (Fig. 1).

2.2. Laboratory setup and experiments

2.2.1. The setup. The Mars Organic Matter Irradiation and Evolution (MOMIE) setup is designed to study the photochemical degradation of organic molecules under Mars-like UV conditions. A scheme of this device is presented in Fig. 2. This setup was entirely described by Poch *et al.* (2013).

The reactor contains the sample, and conditions relevant to the surface of Mars are reproduced. It is cooled at the mean temperature (218 ± 2 K) at the martian surface using a cryostat, and the reactor is pumped down at the mean pressure of 6 ± 1 mbar of pure N_2 (Linde, ≥99.995 vol %). As carbon dioxide atmosphere does not influence the UV photochemistry (ten Kate *et al.,* 2006), we chose to work with N_2

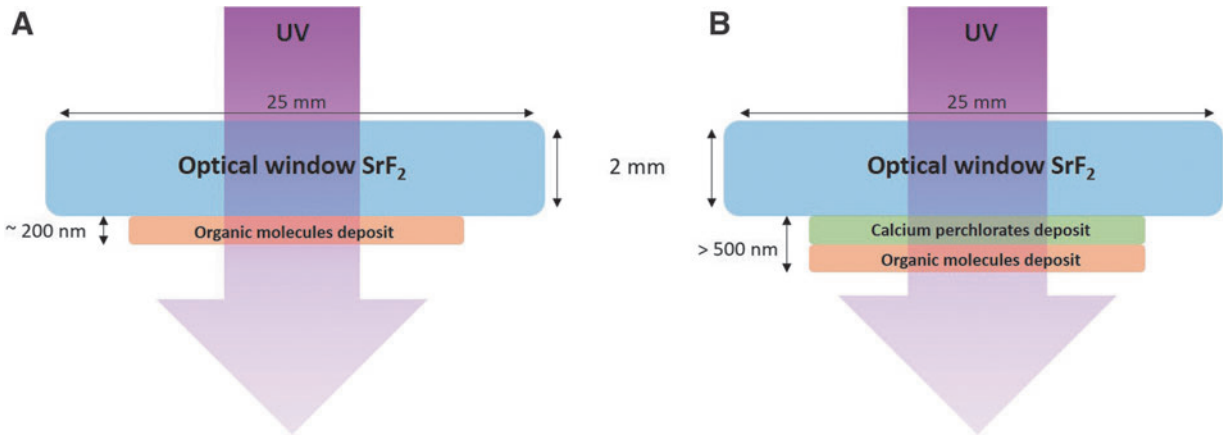

FIG. 1. Schematic representation of samples containing an organic deposit (**A**) compared to sample containing an organic deposit and a calcium perchlorate deposit (**B**).

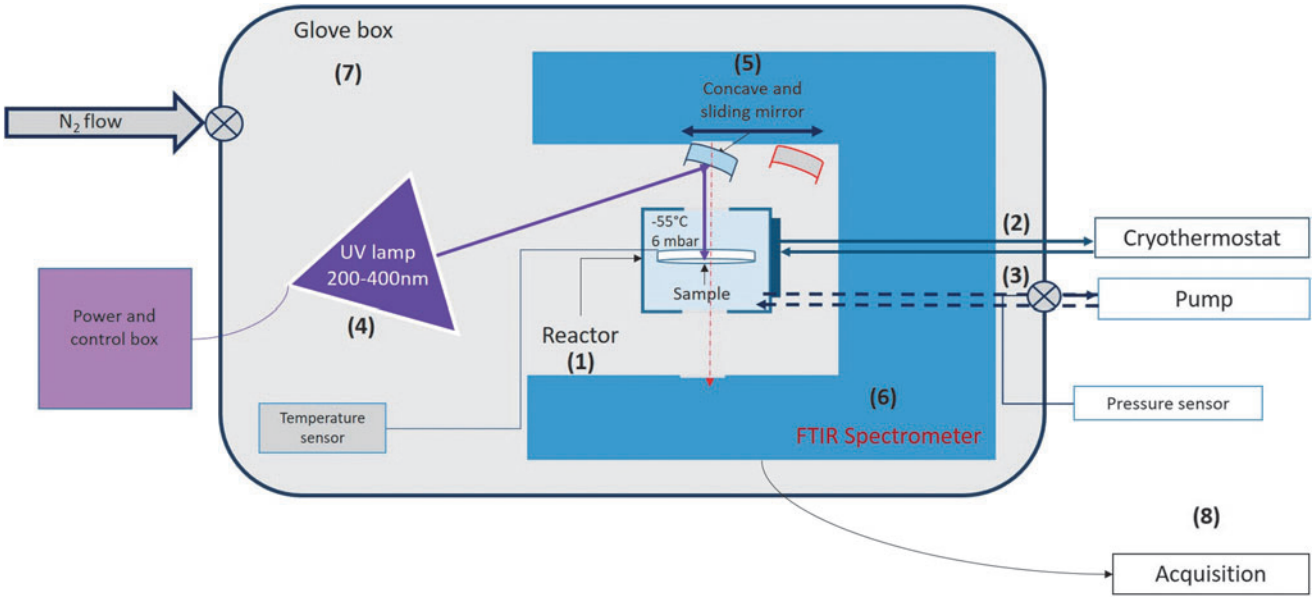

FIG. 2. Schematic representation of the MOMIE setup (Svensson *et al.,* 1999). (1) The reactor containing the sample. The reactor is connected to a cooling (2) and pumping (3) system to keep it at the mean pressure and temperature of the martian surface. The irradiation source is a UV lamp (4) that emits photons in the range of 200–400 nm wavelength. The UV photons emitted by the lamp (purple arrow) are reflected back to the sample by a sliding mirror (5). Analytical monitoring of the sample is carried out by FTIR spectrometry (6) after sliding the mirror (red dotted arrow). The entire device is contained in a glove box (7) and purged and maintained in slight overpressure of dinitrogen. Data acquisition is performed by the Spectrum software (8).

as an inert gas. This also prevents any atmospheric water from interacting with the surface of the sample. The UV radiation reaching the surface of Mars is mimicked by using a Xenon arc spectral lamp (UXL-150SP from LOT-ORIEL) that emits UV photons in the 200–400 nm wavelength range.

Throughout the experiment, the chemical composition of the sample is monitored with an IR spectrometer (Spectrum 100 from Perkin Elmer) with a 4 cm^{-1} resolution in the 4000–800 cm^{-1} spectral range. To prevent gaseous ozone and water ice formation in the setup, the whole experiment is placed in an overpressurized glove compartment purged with dinitrogen (N_2) (Linde, ≥99.995 vol %).

The sample is placed in the reactor, which is sealed with two SrF_2 optical windows that transmit UV light and IR photons. After the reactor is placed in the N_2-purged simulation chamber, it is pumped and cooled to martian conditions for 24 h. It enables assessment of its stability and any sublimation and/or degradation of the sample prior to irradiation.

Before starting the UV irradiation, an IR spectrum is recorded that corresponds to the initial state of the sample (named 0 minutes). The UV exposure time between two IR spectra is usually short at the beginning of the experiment and is increased gradually depending on the evolution of the sample. As a result of the irradiation and the analytical modes of the MOMIE setup, a typical experiment alternates UV exposure and IR analysis, which provides regular monitoring during the experiment.

2.2.2. UV flux characterization and monitoring. The characterization of the flux of the UV lamp is essential to compare the results from each experiment and extrapolate the kinetic data to UV flux received at the surface of Mars. The irradiance received by the sample in the MOMIE setup was measured *in situ* in the 200–400 nm range using transportable UV spectrometer (Black Comet C50, StellarNet Inc., USA). Using this data along with the transmission of SrF_2 windows and the reflectance of the mirror, it is possible to calculate the UV flux exposition of the sample. The spectral range of interest for the study of nucleobases is 200–290 nm, which is the maximum UV absorption zone of uracil samples (see Section 2.3.1).

The first *in situ* data of the UV photon flux that reaches the surface of Mars were made by the REMS instrument on board the Curiosity rover. Curiosity's REMS instrument measures the total irradiance received at the surface of Gale Crater over several days in the UVA, UVB, and UVC ranges (200–380 nm). This total irradiance varies as a function of the diurnal cycle from 0 $W \cdot m^{-2}$ at night to 21 ± 1 $W \cdot m^{-2}$ at noon, but also as a function of the opacity of the atmosphere during dust storms (Haberle *et al.,* 2014). Note that the Curiosity rover and thus the REMS instrument are not at the equator but at latitude 5.4°S and 137.7°E in the Aeolis Mensae region. Since then, REMS performed several measurements of the UV flux, generating data that need, however, to be corrected due to atmospheric dust deposition on the instrument's UV detector. These corrected data are in good agreement with the first REMS measurements made during the first 100 sols of the mission when dust deposition was lower and, thus, did not yet affect the measurements. If one compares the measured UV flux to the flux predicted by the model (Patel *et al.,* 2002) in conditions relatively close to the measurement conditions, it can be seen that this flux can be overestimated by the models. Today, REMS data are the most representative of the flux at the surface of Mars and

Table 2. Variability of the UV Flux of Photons Delivered by the Lamp Reaching the Sample in the Range 200–290 nm

	UV flux ($W \cdot m^{-2}$)
MOMIE 2018 (200–290 nm)	9.49 ± 1.90
MOMIE 2021 (200–290 nm)	1.44 ± 0.29
MOMIE 2022 (200–290 nm)	0.70 ± 0.14
Mars 0° (Patel *et al.,* 2002) (190–290 nm)	2.26
Mars 4,6°S (REMS, MSL) (190–290 nm)	~ 1.24

The UV flux values are compared with those estimated by the model (Patel *et al.,* 2002) and the one potentially received on the surface of Mars in the same wavelength range at the MSL mission landing site. This value is calculated based on the measurement/model ratio.

can be used to improve the radiative transfer models of the atmosphere of Mars (Vicente-Retortillo *et al.,* 2020).

As the extrapolation of the experimental kinetic results requires that the UV flux in the absorption UV range (200–290 nm) is known, we calculated the total energetic flux ratio between the measurements on Mars (22 $W \cdot m^{-2}$ [Vicente-Retortillo *et al.,* 2020]) and the model (~ 40 $W \cdot m^{-2}$ [Patel *et al.,* 2002]). This ratio is equal to 0.55, which enables estimation that the 200–290 nm mean UV flux that reaches the surface of Mars is about 1.24 $W \cdot m^{-2}$. This value was compared to the UV flux received by the sample, which was measured regularly between the different experiments (Table 2). The UV flux decreases over time because of the aging of the optics.

2.3. Sample analysis and characterization before, during, and after the simulation experiment

Before starting an experiment, each sample was analyzed by IR and UV spectroscopy. This allowed for identification of the molecular functions, estimation of the film thickness, and evaluation of UV absorption of the studied molecule. During the experiment, the sample was analyzed regularly by IR spectroscopy to monitor the evolution of the sample for each exposure time (t in minutes). Photoproducts formed by the photolysis of uracil in presence of calcium perchlorate were characterized by UHPLC-HRMS analyses. Results were compared with previous experiments exposing pure uracil in Mars-like conditions (Rouquette *et al.,* 2020), which produced uracil dimers.

2.3.1. UV spectroscopy analysis. UV transmission properties of the studied samples were investigated within the 200–400 nm spectral range with a UV-visible spectrometer (Cary 60 Uv-Vis, Agilent Technologies). Spectra were recorded from 1 scan at 120 $nm \cdot min^{-1}$ with a resolution of 1 nm. As shown in Fig. 3, minimum UV transmission range occurs between 290 and 200 nm with two minima at 200 and 260 nm. This spectral range was used for calculation of the UV flux (200–290 nm) that reached a sample during the irradiation experiment. If UV transmission is higher than 90%, the sample is considered optically thin, which means that all molecules of the sample are irradiated at the same time with the same flux. UV transmission spectra of uracil and [perchlorates + uracil] samples (Fig. 3) are below 90%. Therefore, the samples are not considered optically thin. The presence of perchlorates in the samples increases the thickness and, hence, an even lower transmission of UV photons. The number of UV photons that reach the sample in the same range, as determined by using the measured UV flux (see Section 2.2.2), is multiplied by the transmission of the sample. Therefore, by knowing the number of photons transmitted, it is possible to calculate the number of photons absorbed by the sample.

2.3.2. IR spectroscopy analysis.

- Nucleobase samples:
  For validation and characterization of the samples after their handling, they were analyzed with a Fourier

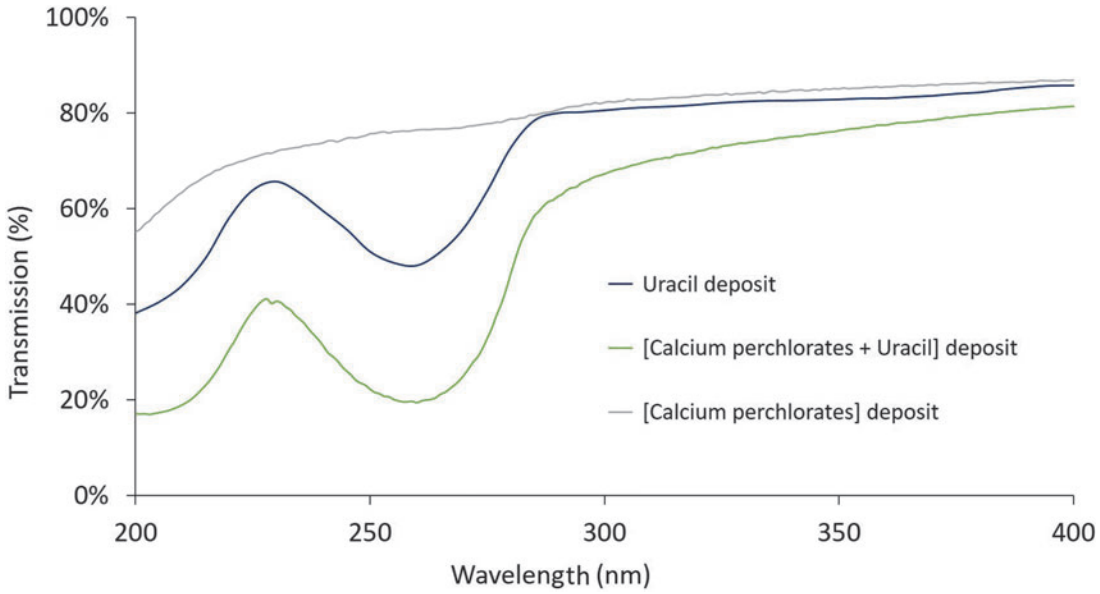

FIG. 3. UV transmission spectra of a calcium perchlorate sample, uracil film with and without perchlorates all deposited on SrF_2 optical windows.

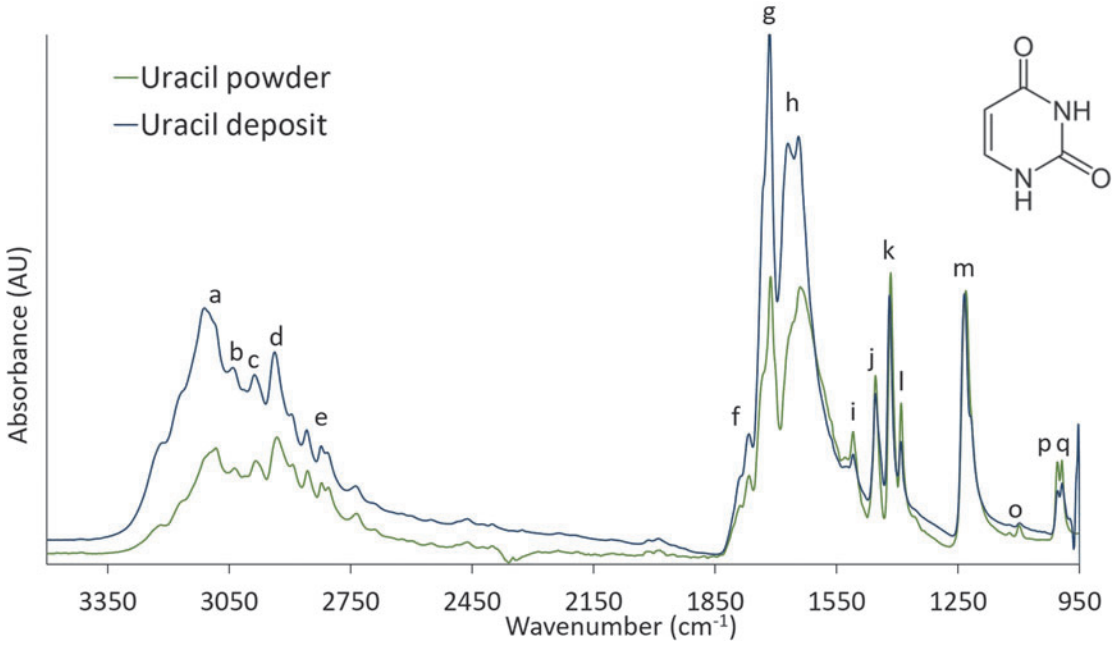

FIG. 4. Qualitative comparison of the IR spectrum of uracil powder (green curve) with the spectrum of uracil deposit (blue curve). This shows that the sample preparation procedure does not degrade the nature of the molecule.

transformation infrared (FTIR) spectrometer (Bruker, 4000–400 cm^{-1}, resolution: 4 cm^{-1}, 35 scans). The initial solid powder of the organic molecule and/or calcium perchlorate was analyzed with the same instrument coupled to an attenuated total reflectance (ATR) system. The IR spectra of the samples were compared with the powder spectra and the IR NIST database (Susi and Ard, 1971; Florián and Hrouda, 1993) in order to validate the sample preparation by basically checking to discern whether there was no significant change in the spectrum (Fig. 4). Attribution of the IR bands characteristic of uracil (Table 3) enables confirmation as to whether the sample handling procedure did not alter the compound before sublimation.

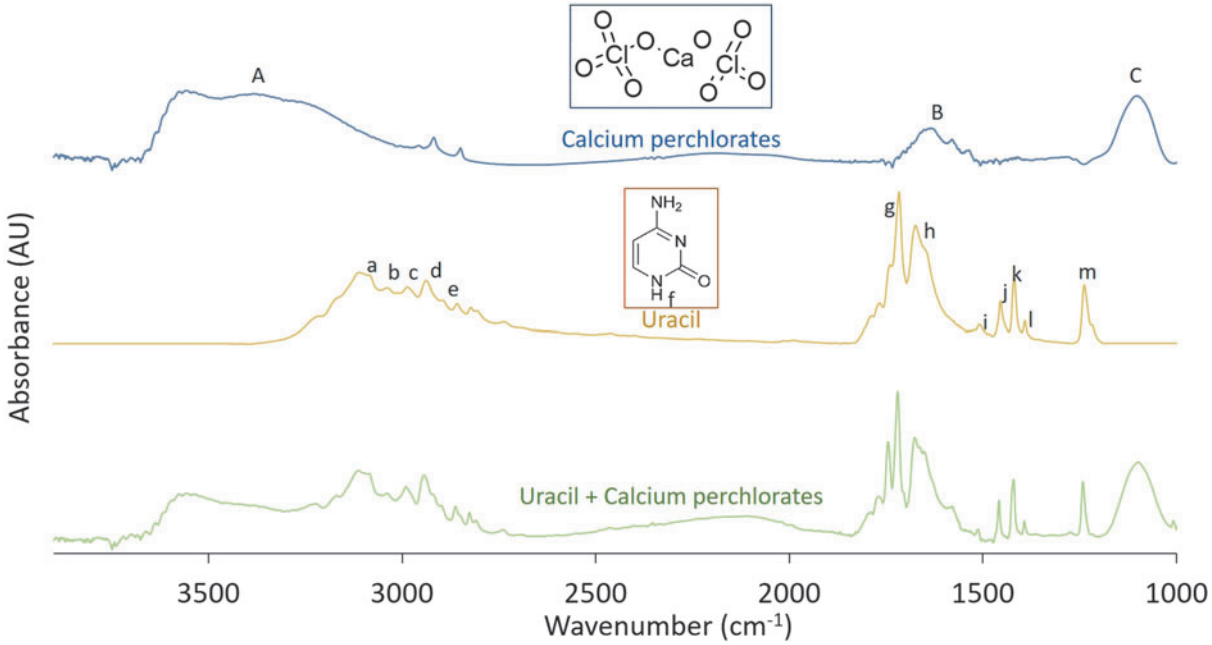

FIG. 5. Comparison of the IR spectra of a calcium perchlorate sample (blue curve), uracil sample (yellow curve), and [uracil + calcium perchlorate] sample (green curve). Baselines of the spectra were shifted for a better reading of the graphic.

Table 3. Uracil IR Characteristic Bands Identification Found in Susi and Ard (1971), Florián and Hrouda (1993), and IR Band Identification of Calcium Perchlorate Sample (Lewis *et al.,* 1975; Kopitzky *et al.,* 2002; Chen *et al.,* 2004)

Molecule	*Label*	*Wavenumber (cm^{-1})*	*Band identification*
Uracil	a	3160–3100	ν_s (Svensson *et al.,* 1999)
			-ν_{as} (Svensson *et al.,* 1999)
	b	3080	ν(CH)
	c, d, e	3000–2850	ν (CH), ν (Svensson *et al.,* 1999)
	f	1790	ν(C=O)
	g	1716	ν(C=O)
	h	1675–1640	ν(C=C)
	i	1508	δ (Svensson *et al.,* 1999)
	j	1453	ν-ring
	k	1417	δ (Svensson *et al.,* 1999)
	l	1390	δ(CH)
	m	1238–1217	ν-ring, δ(CH)
	o	1099	ν-ring
	p	1003	ν-ring
	q	992	δ-ring
Calcium perchlorate	A	3800–3000	ν OH(H_2O)
	B	1635	δ OH (H_2O)
	C	1095	ν_3 (ClO_4^-)

- Nucleobases with perchlorate samples:
  The samples of [uracil – calcium perchlorate] analyzed with FTIR spectroscopy showed that there was no chemical reaction between the calcium perchlorate deposit and uracil during the sample handling. Figure 5 shows a comparison of the IR spectra obtained for (i) a pure uracil sample, (ii) a pure calcium perchlorate deposit, and (iii) a calcium perchlorate and uracil deposit. The spectrum resulting from the [calcium perchlorate + uracil] sample is a combination of both compounds' spectra. This shows that both compounds are present unambiguously in the sample. As no new IR band was observed, we concluded that no new chemical species was produced during the deposition process.

2.3.3. Thickness estimation. Knowing the thickness of the samples is necessary to estimate the number of molecules in the sample before and after exposing it to the Mars-like environment. The number of degraded molecules throughout the experiment enabled calculation of the quantum photodecomposition efficiency of the targeted molecule (see Section 2.4.3). Sample thickness of organic films can be measured after the organic film is deposited by interferometry (WYKO NT1100 Optical Profiling System by Veeco). The thickness of the organic film is proportional to the IR absorbance of the molecular bands. A calibration line was previously calculated by Saïagh *et al.* (2015) to correlate the thickness of uracil films to the IR absorbance of its characteristic bands. This calibration was also used by Rouquette *et al.* (2020) to estimate sample thickness and deduce the number of uracil molecules present in a sample before and after exposure to radiative Mars-like conditions. The samples analyzed in the present study were prepared with this same method and under the same conditions. Therefore, we used the IR absorbance of the samples before irradiation and the correlation curve to estimate the thickness of the uracil film deposited on the calcium perchlorate layer.

The IR absorbance specific to uracil is calculated by subtracting the IR integrated area of the A band ($CaClO_4$) before the uracil deposit to the IR spectrum of the [uracil + calcium perchlorate] sample. Therefore, the IR absorption of uracil in the sample is calculated such that it could be used in a thickness calculation. The calculated thickness of each sample studied in this work is presented in Table 4. The uncertainty of the thickness is calculated according to the work of Saïagh *et al.* (2015).

2.3.4. Ultra-high-performance liquid chromatography–high-resolution mass spectrometry analyses. To identify

Table 4. Thickness of Uracil in the [Calcium Perchlorate + Uracil] Samples, Their Total UV Exposure Time and the Associated UV Flux Received at the Top of the Sample

Sample reference	*Date*	*Thickness (nm)*	*Cumulative exposure time to UV radiation (h)*	*UV flux received at the top of the sample ($W \cdot m^{-2}$)*
CaPerchlo Ura 1	May, 2018	**390** ± 195	**25**	**9.49** ± 1.90
CaPerchlo Ura 2	December, 2020	**290** ± 145	**197**	**1.44** ± 0.29
CaPerchlo Ura 3	January, 2021	**236** ± 118	**271**	**1.44** ± 0.29
CaPerchlo Ura 4	May, 2022	**317**± 158	**67**	**0.69** ± 0.14

potential new compounds that formed during the experiments, solid samples were analyzed by UHPLC-HRMS. Analyzed samples included non-exposed (uracil, and uracil with calcium perchlorate) and samples exposed to UV irradiation (uracil with calcium perchlorate).

The solid samples were solubilized in a mixture of ultrapure water and acetonitrile (ULC/MS – CC/SFC, Biosolve) with an 80:20 volume ratio. Analyses were performed using an ACQUITY UPLC I-Class (Waters) liquid chromatographic system coupled to a Vion-IMS-Q-TOF (Waters) mass spectrometer equipped with an electrospray ionization source. The Vion combines the performance of ion mobility and Q-TOF mass spectrometry for high measurement quality with routine resolution >30,000 (positive and negative ions), an accuracy of 2 ppm on exact mass measurements and 2% on CCS (Cross Collision Section, provided by ion mobility) measurements. The analyses were performed in reverse phase, on an Acquity UPLC BEH C18 2.1 mm × 100 mm, 1.7 µm (Waters) column equipped with a pre-column (ACQUITY UPLC BEH C18 VanGuard 130Å, 1.7 µm, 2.1 mm × 5 mm hybrid, Waters). Gradient elution was carried out by using ultrapure water and acetonitrile (ULC/MS – CC/SFC, Biosolve) as solvents. Formic acid (0.1%) was added to each solvent (99% ULC-MS, Biosolve). The gradient started at 98% of ultrapure water and was increased gradually to 98% of acetonitrile within 25 min. The detection was acquired in positive mode (ESI+) in the 50–1000 *m/z* range. Blank SrF_2 windows are references for all analyses. The calibration is done by using a commercial mixture (Major Mix, Waters) in the positive mode. The mass calibration is done on 15 compounds in the range 50–1000 *m/z* and the calibration in CCS (ion mobility) on 16 compounds.

2.4. Data treatment and kinetic parameters determination

2.4.1. Photolysis rate and half-life estimation. The IR analysis along the irradiation experiment enables monitoring of the uracil molecule quantity in the sample. The relative absorbance of the infrared bands is calculated for each cumulated time (t) from equation (Svensson *et al.,* 1999):

$$\frac{A_t}{A_0} \qquad \text{(Svensson } \textit{etal.}\text{, 1999)}$$

with A_t = area of the infrared bands at a certain time (t) of irradiation, and A_0 = area of the peak before any irradiation ($t = 0$ min).

As the number of molecules is proportional to the area of the absorption bands, this ratio is proportional to relative abundance of molecules following Equation 2:

$$\frac{A_t}{A_0} = \frac{N_t}{N_0} \qquad (2)$$

with N = the number of molecules. By monitoring the relative abundance of molecules in the sample during the experiment, it is possible to determine the half-life ($t_{1/2}$ in [time]) and photolysis rate (J in $[\text{time}]^{-1}$) of uracil molecules in these experimental conditions. However, the measurements of $t_{1/2}$ and J closely depend on the thickness of the samples that are not precisely controlled during the handling. Moreover, the calculation of these two kinetic parameters is only relevant for optically thin samples as it was stated by Poch *et al.* (2013). However, half-lives were observed experimentally and were also theoretically calculated considering a zero-kinetic order plotted from the average A_t/A_0 as a function of the exposure time. Therefore, these values have been determined from experimental data and extrapolated to the surface of Mars as an estimation, although they present a high percentage of uncertainty due to the thickness variations between samples.

From the UV spectral irradiance measurements received by a sample in the MOMIE setup (Section 2.2.2), we can then calculate the energy flux of the photons that reach the surface of the sample. Knowing this flux, the kinetic data were extrapolated to the surface of Mars according to Equation 3:

$$t_{\frac{1}{2}}(\text{Mars}) = t_{\frac{1}{2}}(\text{MOMIE}) \times \frac{\text{Flux}_{\text{MOMIE}}\ (200-290\ \text{nm})}{\text{Flux}_{\text{Mars}}\ (200-290\ \text{nm})} \qquad (3)$$

2.4.2. IR band deconvolution. To follow the relative absorbance of uracil, Rouquette *et al.* (2020) studied the IR band labeled ''m'' (Table 3) assigned to the cycle stretching and plotted its equation (Svensson *et al.,* 1999) as a function of the exposure time. Results suggest that new IR bands that formed during the irradiation would contribute to absorption in the monitored wavenumber range. Thus, the integration treatment of the areas of these bands can present high uncertainties. This was also observed in the present study as new IR bands were formed along the experiments, overlapping with the targeted band (Fig. 6). To avoid this bias, the area of this same targeted band ''m'' was determined after deconvolution of the spectra in the wavenumber range 1330–1180 cm^{-1}, taking into account only the area of the initial ''m'' band and removing the contribution of newly formed band(s). The ''Peak-deconvolution'' app in the OriginPro-2020 software was used to carry out the deconvolution. The peak search was performed by choosing a constant baseline then using a second derivative method with a Savitzky–Golay filter and a Gaussian pointing. The tolerated upper limit of the χ^2 value was set at 10^{-6}. With these parameters, the fitting results were plotted as deconvoluted spectra and compared to the original spectra (Fig. 7).

2.4.3. Quantum photodecomposition efficiency. The experimental quantum photolysis efficiency Φ_{exp} (in molecule·photon^{-1}) is calculated to overcome the influence of the film thickness and to compare quantitatively the degradation rate of uracil in all the samples. This requires knowing how many photons were absorbed by the sample during a complete experiment in the range of 200–290 nm where uracil absorbs UV photons. This information is provided by measurement of the lamp UV flux (Section 2.2.2). If the number of molecules present in the sample is known (deduced from thickness data), the quantum photolysis efficiency Φ_{exp} can be calculated with Equation 4:

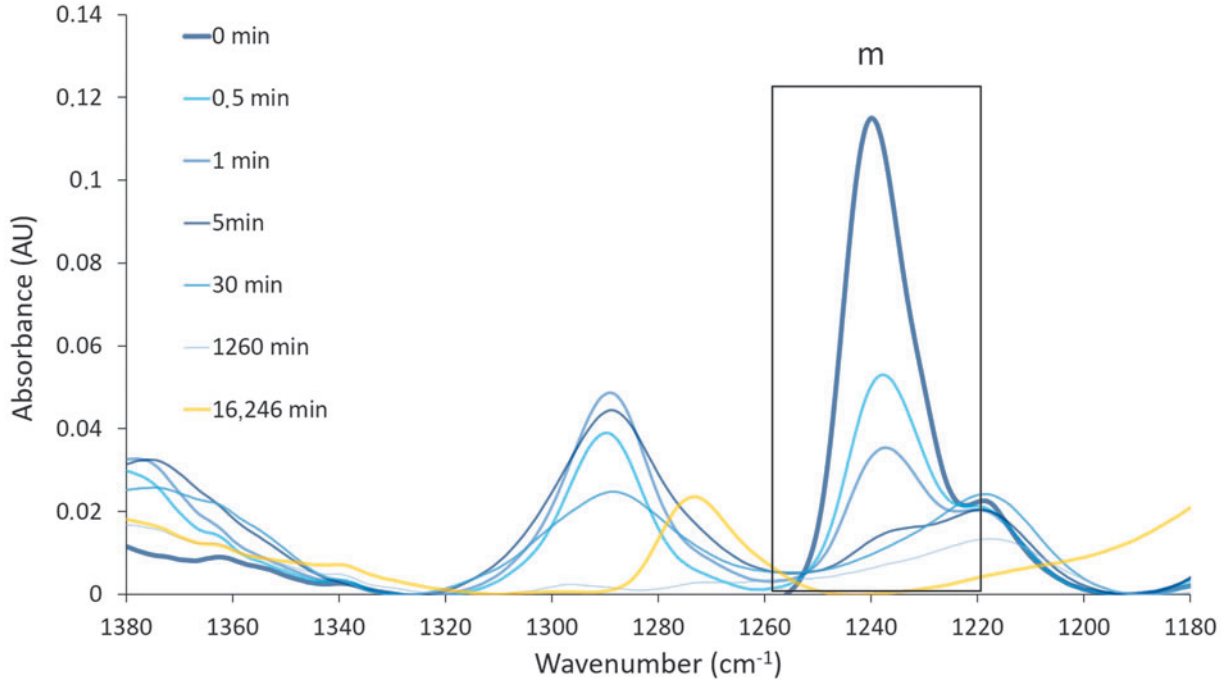

FIG. 6. Evolution of the uracil IR characteristic band (ν-ring) ''m'' during the simulation. Blue thick line: initial spectrum (t_0). Yellow thick line: final spectrum. Other blue lines: intermediate spectra. The band labelled ''m'' is the band used to follow the kinetic degradation of the amount of uracil within time exposure. Along the irradiation experiment, other bands are formed and overlapped with the ''m'' band.

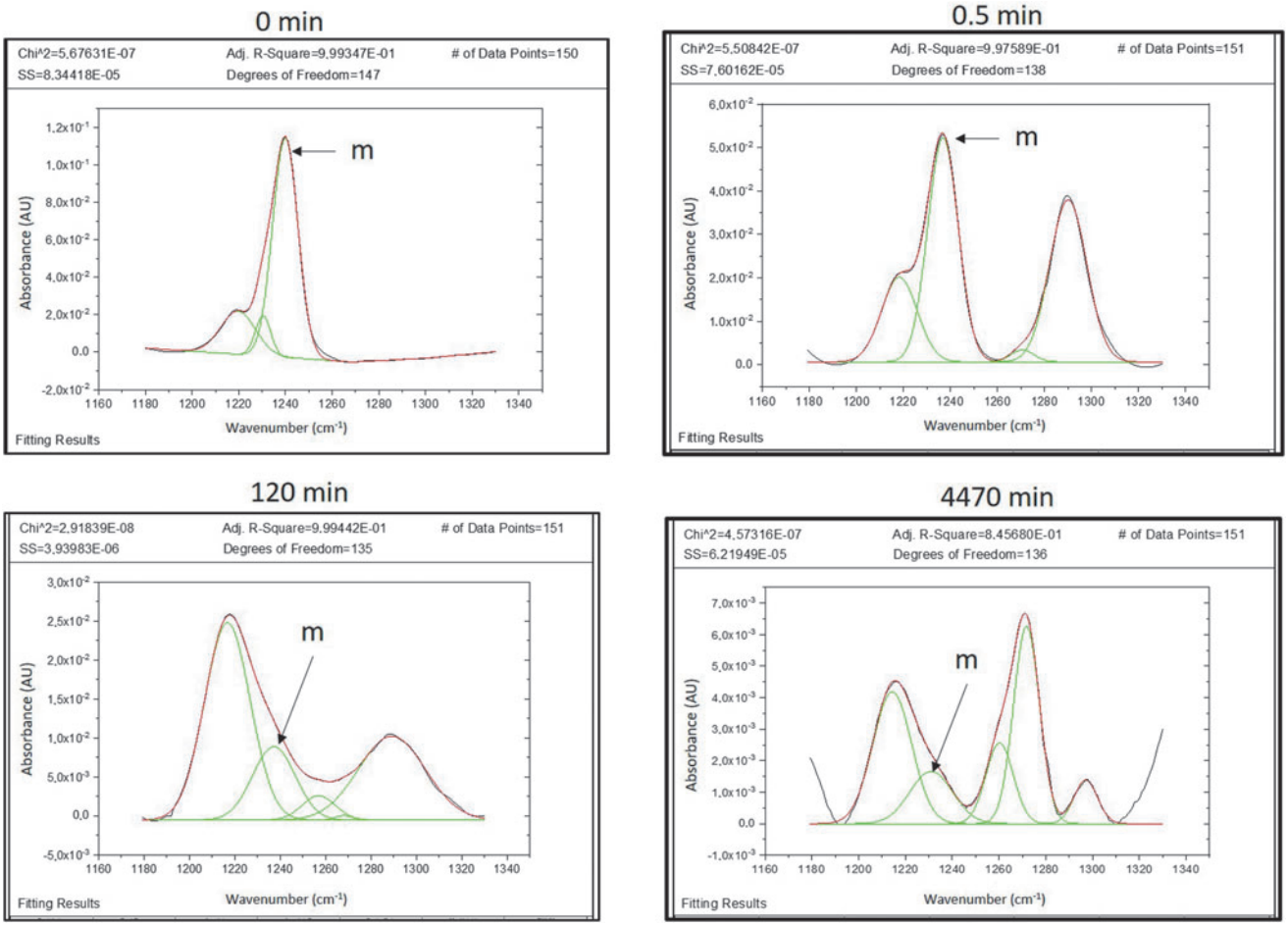

FIG. 7. Deconvolution of the IR spectrum of a [uracil + calcium perchlorate] sample in the 1330–1180 cm^{-1} range at different irradiation times. This method enabled to follow the evolution the band labeled ''m'' corresponding to the uracil cycle stretching. With the exposure time increasing, new IR bands appear and/or increase, overlapping with the ''m'' band.

$$\Phi_{\text{exp}} = \frac{\text{number of degraded molecules}}{\text{number of photons absorbed}} \quad (4)$$

The number of molecules present in the sample at any time of the experiment (N_t) is calculated with Equation 5:

$$N_t = N_a \times \frac{e_t \times \pi r^2 \times \mu_{\text{ura}}}{M_{\text{ura}}} \quad (5)$$

where N_a is Avogadro's constant (mol^{-1}), e_t is the sample thickness (m) for a known time (t) of the experiment, r is uracil deposit radius (m), μ_{ura} is uracil volumetric mass density ($\text{g}\cdot\text{m}^{-3}$), and M_{ura} is uracil molar mass ($\text{g}\cdot\text{mol}^{-1}$).

Therefore, the quantum photolysis efficiency can be calculated with Equation 6:

$$\Phi_{\text{exp}} = \frac{N_0 - N_t}{\int_0^t F_{200-290}} \quad (6)$$

where Φ_{exp} is the experimental quantum photolysis efficiency ($\text{molecule}\cdot\text{photon}^{-1}$), N_0 is the number of molecules in the sample before any irradiation, N_t is the number of molecules in the sample after an irradiation time t, $F_{200-290}$ is photon flux in the range 200–290 nm ($\text{photons}\cdot\text{s}^{-1}$).

3. Results

3.1. IR spectroscopy

The study of the uracil IR spectra over time shows that this molecule is quickly degraded within the first seconds of exposure (Fig. 8). Indeed, characteristic bands of uracil decrease continuously with the irradiation time. The formation and/or increase of new bands indicates that new chemical functions are produced. These significant changes of the IR spectra obtained at different exposure times are evidence of a specific reactivity of uracil submitted to UV irradiation in the presence of calcium perchlorate.

To identify more precisely the different IR bands that are formed during the experiments, we subtract a spectrum obtained at a given irradiation time (t) to the spectrum obtained before any irradiation (t_0). From this resulting spectrum, IR bands with negative values represent decreasing absorption bands, meaning the corresponding chemical functions are less present than before irradiation. Conversely, IR bands with positive values represent new IR absorption bands that were absent before irradiation. These new chemical functions, formed during UV exposure, could belong to intermediate compounds (Fig. 9) and/or to new, more stable photoproducts (Fig. 10).

Figure 9 shows the IR spectra of a sample of uracil and calcium perchlorate during the first 120 min of irradiation. In a first phase, we observe new IR bands (labeled 1 to 9 in Table 5) that are formed within 5 min of UV exposure and decrease after this time. This indicates that intermediate photoproducts are formed. Most of these new bands are common to those formed during the experiments when exposing pure uracil to the same conditions as indicated in the work of Rouquette *et al.* (2020) with the exception of band 6 (assigned to ν O-H). Over a second phase, new bands (labeled 10 to 15 in Table 5) appear and persist for more than 8000 min (Fig. 10). This is interpreted as the formation of photoproducts more stable than uracil itself, as formerly

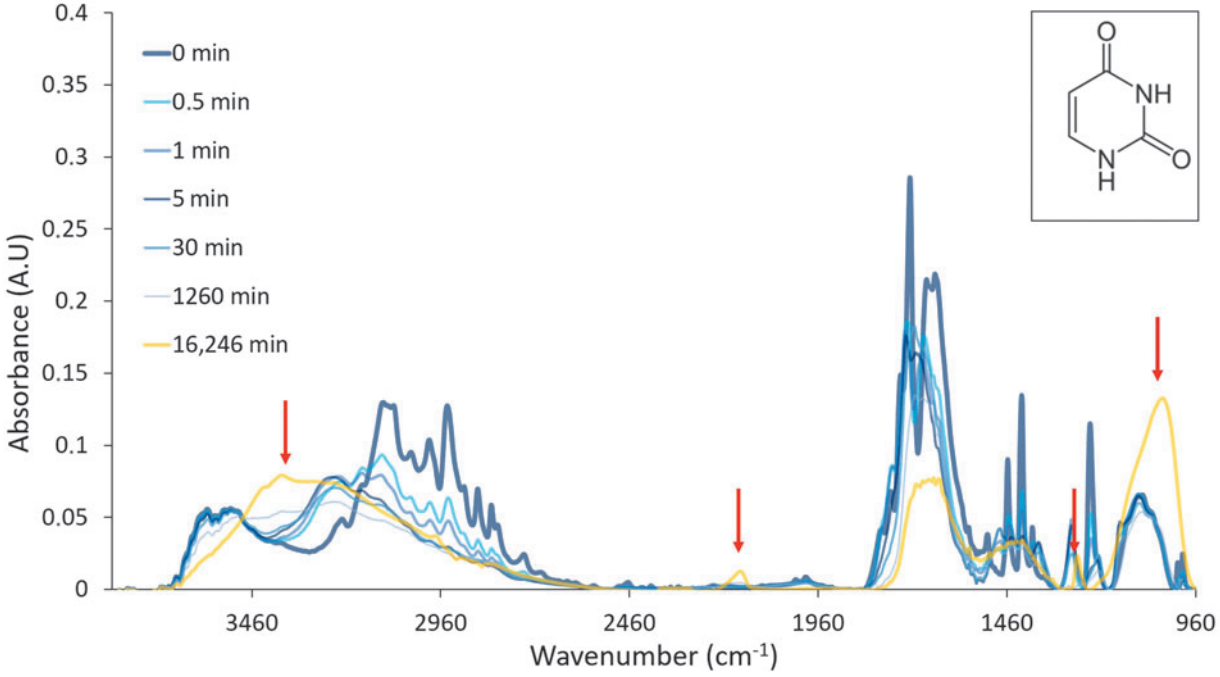

FIG. 8. Superposition of IR spectra corresponding to a sample containing uracil and calcium perchlorate at different times of UV exposure in Mars-like conditions in the MOMIE experiment. The blue thick line corresponds to the initial spectrum (t_0) and the yellow thick line to the final spectrum at the end of the experiment. Many changes in the IR bands are observed within the experiments. Most of the characteristic bands of uracil decrease along the exposure whereas new IR bands appear (identified with red arrows on the figure).

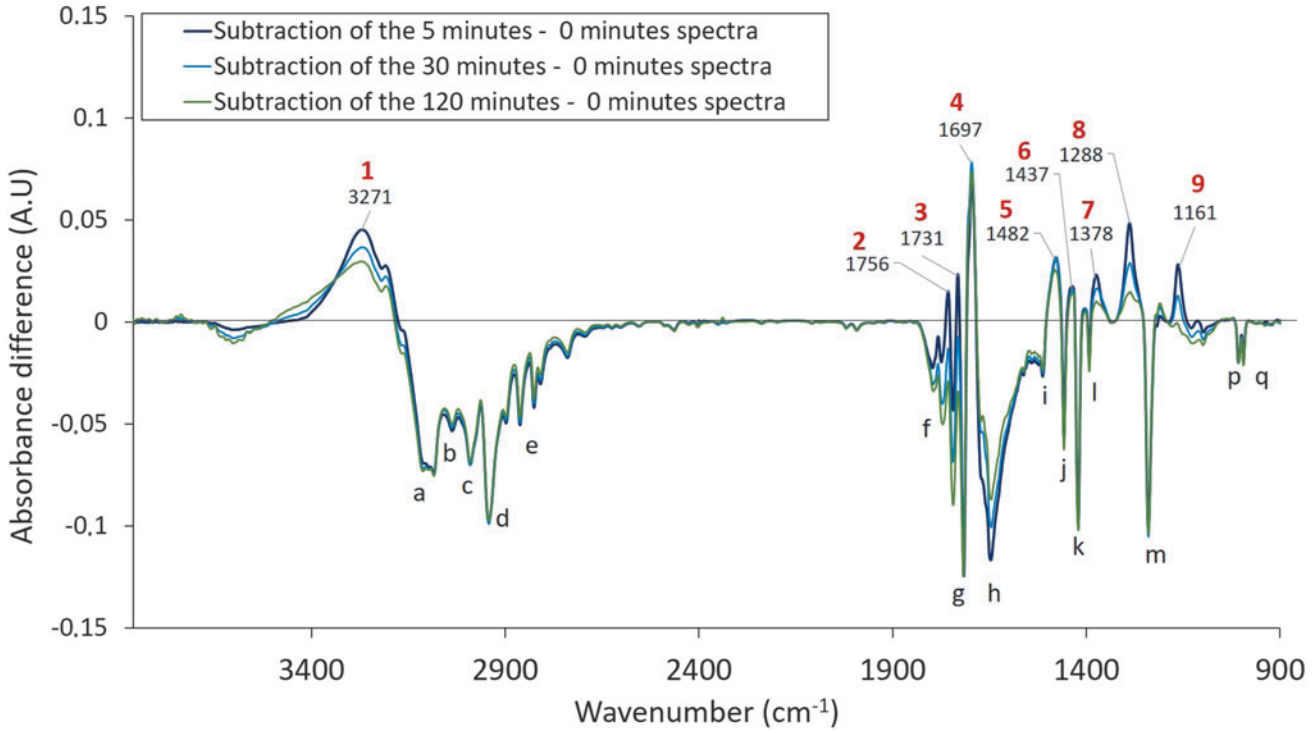

FIG. 9. Subtraction spectra from the first irradiation time exposures: 5 min (dark blue), 30 min (light blue), and 120 min (green). Negative bands correspond to the decrease in intensity of the characteristic bands of uracil. Positive bands, numbered in red, correspond to the bands appearing and increasing in intensity. After 5 min, the intensity of these new peaks decreases with the irradiation time increasing.

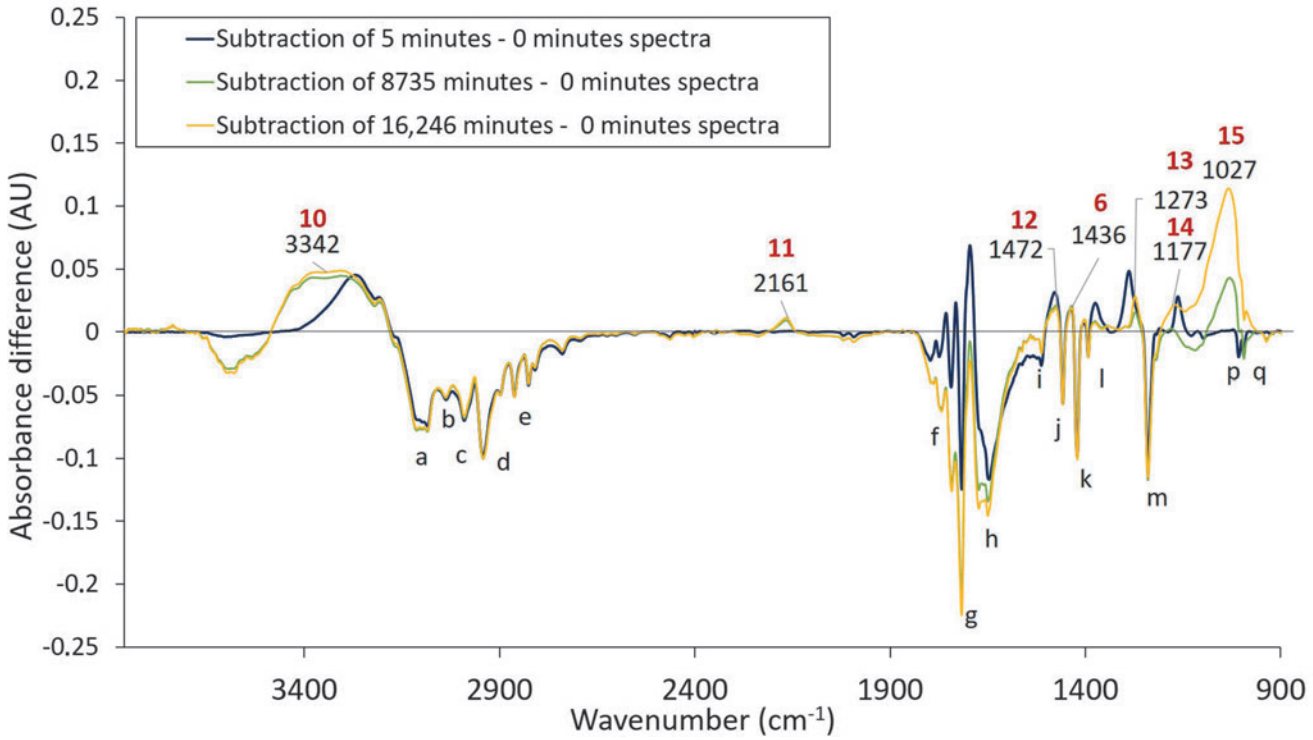

FIG. 10. Subtraction spectra after high irradiation time: 8735 min (light green) and more than 16,000 min (yellow). After 8735 min, the intensity of the new peaks increased until the end of the experiment.

Table 5. Spectral Assignments of the Infrared Absorption Bands of the Products and Comparison with the Results from Pure Uracil Exposure Conditions (Rouquette *et al.*, 2020)

Label	*Wavenumber (cm^{-1})*	*Peak identification*	*Common to pure uracil experiments (Rouquette* et al., *2020)*
1	3271	ν OH	Yes
2	1756	ν C=O	Yes
3	1731	ν C=O	Yes
4	1697	ν C=N and/or ν C=O	Yes
5	1482	ν N-H/δC-H	Yes
6	1437	ν OH	No
7	1378	ν N-H/δC-H	Yes
8	1288	ν C-O and/or ν C-N	Yes
9	1161	ν C-O	N/A
10	3342	ν OH and/or ν NH	Yes
11	2161	ν C≡C or ν C≡N	No
12	1472	δC-H	No
13	1273	ν C-N and/or ν C-O	No
14	1177	ν C-O	No
15	1027	δO-H	N/A

observed during pure uracil irradiation experiments (Rouquette *et al.,* 2020). Most of the chemical functions observed in this experiment are attributed to alkyl, carbonyl, amine, and O-H bearing functions, which is also consistent with those previous results. This indicates that one (or more) photoproduct formed by the photolysis of uracil with calcium perchlorate is likely similar to those formed with pure uracil. The bands labeled 9 (assigned to ν C-O) and 5 (assigned to δ O-H) were not observed by Rouquette *et al.* (2020) because of the use of a different optical window (MgF_2) that absorbs IR light under 1200 cm^{-1}. However, five other bands (labeled 6, 9, and 11 to 14) were not observed by Rouquette *et al.* (2020) either. Most of them are assigned to chemical functions that are commonly present in uracil dimers. However, other compounds may have formed. Indeed, we identified ν C≡C or ν C≡N (band 11) after a long exposure time (more than 8000 min). This coincides with the formation of the band labeled 15 (δ O-H), which might suggest that these two bands (11 and 15) may be associated with the same photoproduct. Also, the band 6 at 1437 cm^{-1} (ν O-H-), present throughout the experiment, associated with the band 10 (3342 cm^{-1}), observed from 240 min of irradiation, is coherent with the presence of carboxylic acids.

The relative absorbance (Equation 1) of the band labeled ''m'' was plotted as a function of the exposure time (Fig. 11). This band was chosen as a comparison of the present results to previous experiments on the degradation of pure uracil in the same experimental conditions (Rouquette *et al.,* 2020). Two trends are observed on the relative absorbance of this band. First, it decreases quickly within the first 10 min of exposure to UV. This shows that uracil is quickly photolyzed to form photoproducts as it was observed in the IR spectra. The second trend is characterized as a very slow decrease of the relative absorbance from 10 min until the end of the experiment. As the area of the band was retrieved by deconvolution, this cannot be explained by the influence of other IR bands formed during the experiments. Therefore, one plausible interpretation is that the photoproducts absorb UV light in the range 200–400 nm, which protects the underlying uracil molecules.

Moreover, it must be noted that uracil films are not optically thin in the UV range at which we proceed to the photolysis. This means that a large fraction of the uracil deposit is not in contact with calcium perchlorates. Therefore, the kinetic trend observed in Fig. 11 might be due to two different photodegradation processes as follows: (i) degradation of UV-exposed uracil calcium perchlorates system and (ii) UV-exposed uracil alone in the layer that is not in contact with calcium perchlorates. However, the main observation is that uracil is photodecomposed much quicker when calcium perchlorates are present in the sample compared to pure uracil films with similar thicknesses. This could be explained by the intermediate products (not identified yet) that might generate a higher chemical reactivity and/or more chemical chain reactions within uracil molecules in the part of the deposit that is not in contact with calcium perchlorates. This is supported by the observation of many IR bands that were not observed during the evolution of pure uracil exposure to UV (Table 5).

Table 6 sums up kinetic results relative to each sample. The half-life ($t_{1/2}$) data were observed experimentally for each experience. Depending on the thickness of the samples, half-life values go from 3 to 7 min with a high uncertainty percentage due to error bars in the thickness estimation and UV flux variability. The theoretical half-life was calculated by using a zero-order kinetics in the first 12 min from the average relative absorption (Equation 1) data plotted as a function of exposure time. Its value was estimated around 4.6 min in the present experimental conditions.

Because the IR spectrum of uracil evolves quickly in the spectral range used for thickness estimation (3400–1900 cm^{-1}), the photoproducts might influence the absorption of uracil in that range. Therefore, the experimental quantum photolysis efficiency of uracil in the presence of perchlorates was calculated from the first 30 s of exposure and was found to be 12.3 ± 8.3 molecule·photon^{-1} with a high uncertainty percentage due to error bars in the thickness estimation and UV flux variability. This experimental quantum photolysis efficiency is much higher (about 42 times) than the one calculated for pure uracil (0.30 ± 0.26 molecule·photon^{-1}) if we consider only the absorbed

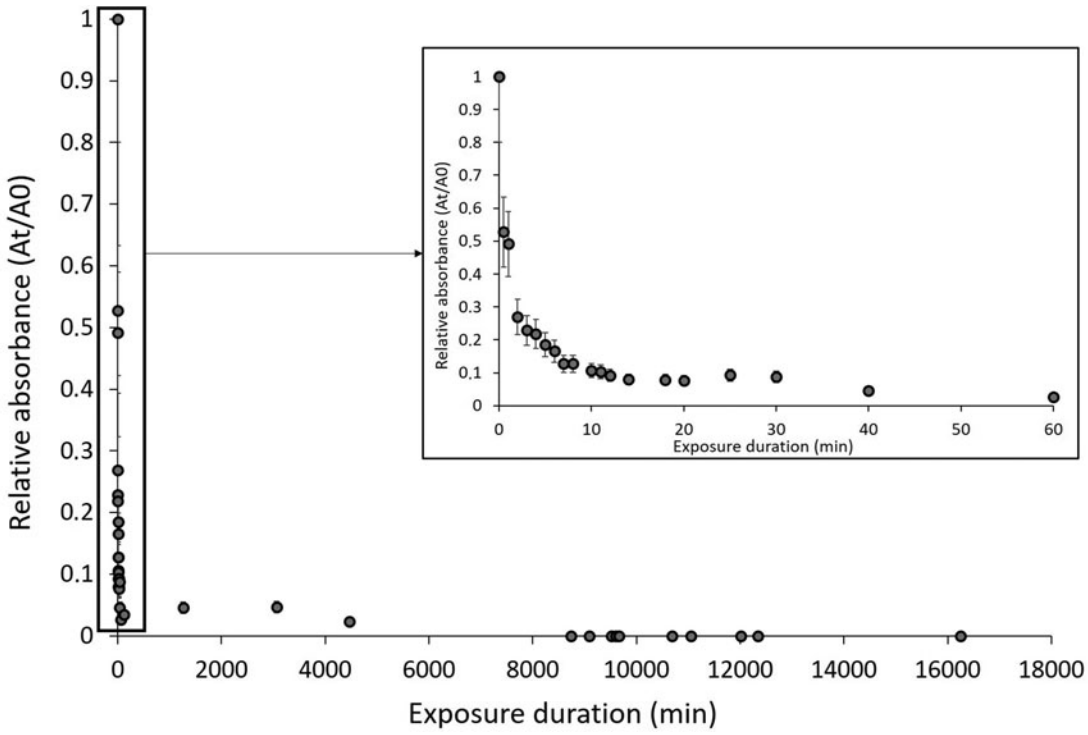

FIG. 11. Degradation of uracil in the presence of calcium perchlorate for 16,000 min in the MOMIE experiment simulating the martian UV environment. The relative absorption (A_t/A_0) of the band labeled ''m'' attributed to the stretching of the uracil cycle is plotted as a function of the exposure time. The error bars are based on the instrumental error (2%) and the uncertainty due to the evolution of the number of photons delivered by the lamp (20%)

photons by the uracil molecules. This suggests that the presence of calcium perchlorate accelerates the photolysis of uracil in Mars-like UV radiative conditions. However, uracil was still detected in irradiated samples for almost 6 days. The constant increase of the relative absorbance of new IR bands suggests that the photoproducts formed by the photolysis of uracil are absorbing UV photons and provide a shielding effect to the underlying uracil molecules. Moreover, the reactivity of these photoproducts could also lead to the formation of secondary products as it was observed in the IR spectra after 8000 min of exposure as stated before.

3.2. UHPLC-HRMS results

Unexposed and exposed samples of uracil and calcium perchlorate samples were analyzed by UHPLC-HRMS. The total exposure time of each sample varied from 400 to 8230 min of irradiation in order to identify potential intermediate photoproducts. The $[M+H]^+$ uracil ion has been detected in all samples with a retention time of 0.677 ± 0.005 min and a *m/z* ratio of 113.0344 ± 0.0001 (Fig. 12). Non-exposed samples did not show any evidence of $[2M+H]^+$, corresponding to uracil clusters of two uracil

TABLE 6. CHARACTERISTICS AND KINETIC RESULTS OF THREE DIFFERENT SAMPLES STUDIED IN THE MOMIE SETUP

Sample	*CaPerchlo Ura 1*	*CaPerchlo Ura 2*	*CaPerchlo Ura 3*	*CaPerchlo Ura 4*	*Uncertainty interval (±)*
Total exposure time (min)	1500	11795	16246	4028	
Experimental half-life ($t_{1/2}$) (min)	7	6	3	7	(±70%)
Initial thickness (nm)	390	353	236	317	(±50%)
Thickness after 30 seconds (nm)	137	164	110	278	(±50%)
Number of degraded molecules during the irradiation time	6.9E+16	3.5E+16	3.4E+16	1.0E+16	(±50%)
Number of photons absorbed during irradiation time (200–290 nm)	1.1E+16	2.5E+15	1.9E+15	1.0E+15	(±20%)
Quantum photolysis efficiency φ (molecule·photon^{-1})	6.4	14.0	18.6	10.2	(±50%)
Average quantum photolysis efficiency φ (molecule·photon^{-1})	12.3				8.3

The half-life of each sample was observed experimentally. The number of degraded molecules was calculated from the thickness of the samples after 30 s of exposure. The quantum photolysis rate was calculated using the number of degraded molecules and the number of UV photons received at the top of the samples (Equation 4) during the first 30 s of exposure.

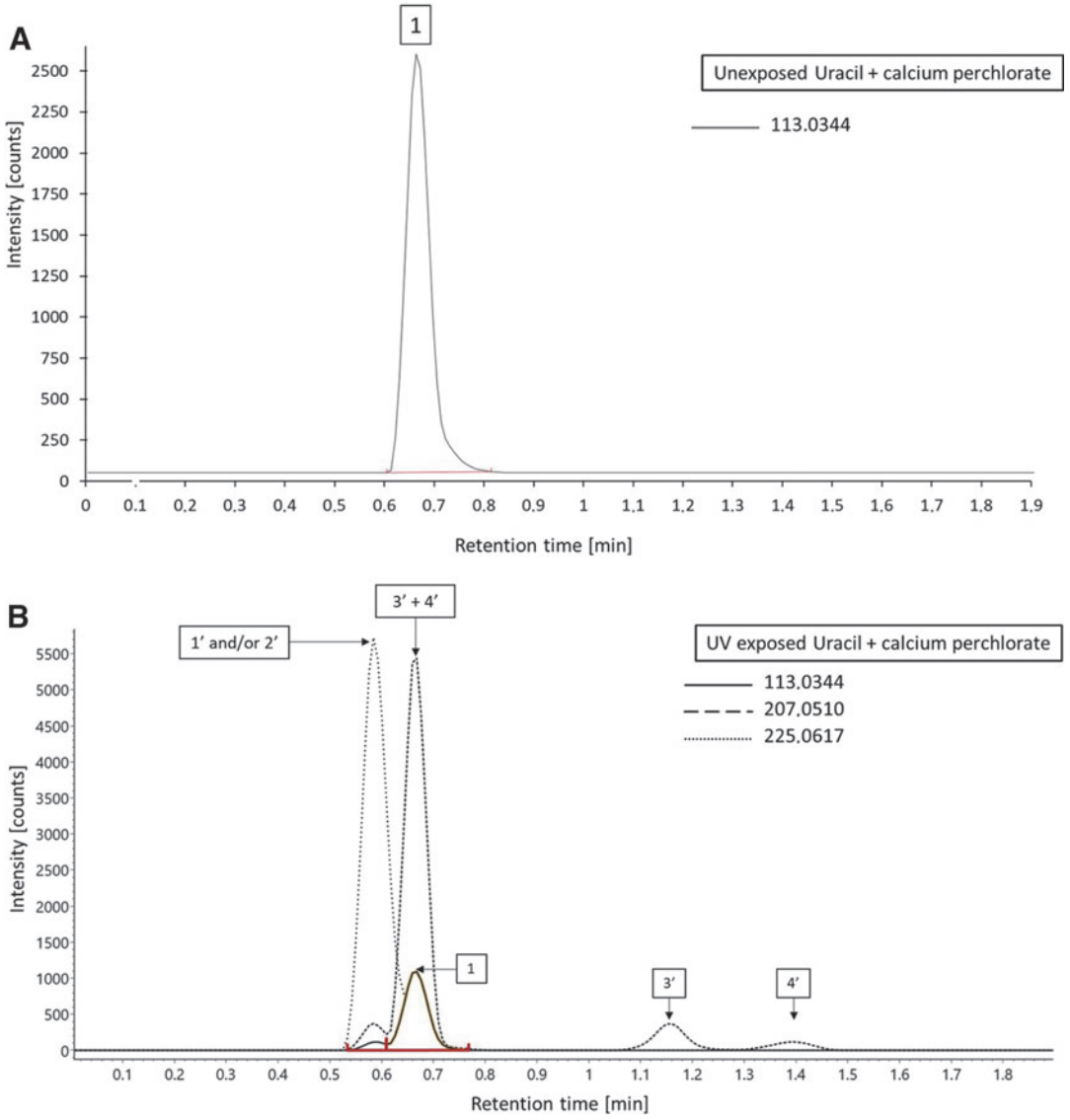

FIG. 12. Chromatograms of two uracil samples: (**A**) an unexposed uracil + calcium perchlorate sample and (**B**) a uracil + perchlorate sample exposed to martian irradiation for 68 h. The exposed uracil samples show four new peaks corresponding to four photoproducts (labeled from 1' to 4'). Peak labeled 1' contributes to ion with *m/z* 225.0620 and peaks labeled 3' and 4' to ion with *m/z* 207.0513. Uracil is also detected in exposed samples, labeled 1.

molecules formed in the instrument, as it was detected in Rouquette *et al.* (2020). On the other hand, exposed uracil samples showed chromatographic peaks attributed to four photoproduct ions, all more intense than the chromatographic peak of uracil (labeled from 1' to 4' in Fig. 12). To identify the dimers, we used the same $[M+H]^+$ ions as Rouquette *et al.* (2020): $m/z = 225.0617 \pm 0.0002$ corresponding to 1' and 2' dimers, and $m/z = 207.0512 \pm 0.0004$ corresponding to 3' and 4' dimers (Fig. 12). Based on their theoretical and experimental masses, the retention times (Table 7) and CCS values of these dimers indicate that multiple forms of these dimers might be present in the samples. Neither uracil nor its dimers have been identified in the blanks (analysis of the empty SrF_2 windows) or in the unexposed uracil sample. The ion spectra of each chromatographic peak are shown in the Supplementary Section Appendix B (Section 7.2).

Only one form of the ion with $m/z = 225.0617 \pm 0.0003$ was detected by chromatography at a retention time of 0.60 ± 0.02 min (labeled 1' and/or 2' in Fig. 12). On the other hand, four other chromatographic peaks were detected for the ion with $m/z = 207.0512$ at different retention times, which implies that both of the forms 3' and 4' might be present in their symmetric (''syn'') and antisymmetric (''anti'') configurations as described by Rouquette *et al.* (2020). However, the software ''UNIFI'' used for the identification of these peaks is not able to differentiate the two forms nor the different configurations insofar as the same characteristics (exact mass, retention time, CCS) are attributed by UNIFI to both syn and anti forms. Their chromatographic peaks were, therefore, attributed to their retention time in the column. These results suggest that 1' and 2' dimers were not separated by chromatography or that

Table 7. Identified Uracil Dimers with Respect to their Retention Time (RT) (After Sorting and Manual Evaluation of the Data)

$[M+H]^+$	*RT (min)*	*CCS (Å²)*	*Identification*
113.0344 ± 0.0001	0.677 ± 0.005	117.3 ± 0.3	1
207.0510 ± 0.0002	0.590 ± 0.005	139.5 ± 0.6	3' and/or 4'
207.0510 ± 0.0002	0.678 ± 0.005	139.7 ± 0.5	3' and/or 4'
207.0512 ± 0.0004	1.164 ± 0.007	140.9 ± 0.6	3'
207.0512 ± 0.0004	1.406 ± 0.007	147.1 ± 1.5	4'
225.0618 ± 0.0003	0.600 ± 0.02	188.8 ± 2.2	1' and/or 2'

the presence of calcium perchlorate in the samples favors the photoproduction of 3' and 4' dimers.

4. Discussion

4.1. Kinetics of photolysis of uracil in the presence of calcium perchlorate on Mars

Photodissociation efficiencies do not require extrapolation of the data to the surface of Mars since they take into account the energy of photons in a precise wavelength range (here, 200–290 nm). Half-lives, on the other hand, are strongly dependent on both the thickness and the UV flux of the photons (expressed in $W \cdot m^{-2}$) received by the sample during the experiment. From the spectral irradiance measurements received by a sample in the MOMIE device, we can then calculate the energy flux of photons that reach the surface of the sample. Knowing this flux, we can extrapolate the kinetic data to the surface of Mars according to Equation 3. This relation implies the need to know the energy flux in the same range on the surface of Mars. As already explained in Section 2.2.2, the UV flux in this range was estimated to be around 1.24 $W \cdot m^{-2}$ (based on *in situ* measurements and theoretical data ratio).

As shown in Table 8 and explained in Section 2.4.1, the half-life time varies according to the thickness of the sample and the UV flux to which the molecule is subjected. Nevertheless, the extrapolated results give an idea of the order of magnitude of the half-life of these molecules on Mars. In the case of uracil, its half-life time on Mars was estimated by Rouquette *et al.* (2020) and would not exceed about 4 h when the molecule is exposed to UV radiation only. In the presence of calcium perchlorate, this half-life time is reduced to only a few minutes. This indicates that their presence favors the photodissociation of uracil and the formation of new photoproducts. Consequently, the presence of uracil in the first centimeters of the surface of Mars seems unlikely due to its rapid degradation when exposed to UV photons especially if it is in contact with calcium perchlorate present in the regolith.

4.2. Identification of photoproducts

Rouquette *et al.* (2020) showed that uracil produces dimers when this molecule is exposed to UV radiation under simulated martian environmental conditions. This resulted in the formation of new IR bands on the spectrum of the molecule during irradiation experiments. In the presence of perchlorates, uracil exposed to UV radiation also produces new compounds. Many of the bands observed during these experiments are common with those observed in the case of pure uracil exposure. This implies that some of the photoproducts formed during irradiation in the presence of perchlorates are similar to those produced in the case of uracil alone. To verify this hypothesis, additional analyses were conducted by another analytical technique (UHPLC-HRMS). Results show that the exposure of uracil in the presence of calcium perchlorates also leads to the formation of uracil dimers. Nevertheless, other bands are observed on the IR spectra that correspond to the evolution of the system [perchlorates + uracil] which were not observed for pure uracil such as triple bonds (C ≡ C and/or C≡N) and C-N and/or C-O simple bonds as described in Table 5. These IR peaks might correspond to one or more new photoproducts that can be formed only in the presence of calcium perchlorate. However, to characterize these new compounds, the chemical pathways toward producing triple bonds from uracil have to be investigated. Indeed, the formation of these triple C ≡ C bonds would require the opening of the uracil cycle and/or the formed photoproducts (dimers for example) accompanied by a rearrangement of the carbon skeleton. It is then highly probable that the primary structure of the

Table 8. Estimated Half-Life of Uracil in Presence of Calcium Perchlorate Extrapolated to Mars Based on the UV Flux (200–290 nm) Calculated in Patel *et al.* (2002) and *In Situ* Measurements (Vicente-Retortillo *et al.,* 2020)

Sample	*Thickness (nm)*	*Experimental Half-life MOMIE (min)*	*Extrapolated to Mars*	
			Half-life Patel, 2002 (min)	*Half-life MSL site (min)*
CaPerchlo Ura 1	**390** ± 195	7	29	53
CaPerchlo Ura 2	**290** ± 145	6	4	7
CaPerchlo Ura 3	**236** ± 118	3	2	4
CaPerchlo Ura 4	**317** ± 158	7	2	4

aromatic cycle disappears, which is supported by the monitoring of the m band, which is representative of the cycle. The opening of the cycle may also be an intermediate step that could lead to a recyclization. In this case, we would go to a cycloalkyne structure with a carbon number greater than or equal to 6. Because of the rigidity of the triple bonds, this type of compound must have a high carbon number to be thermodynamically stable. The most stable cycloalkynes have a carbon chain of more than 8 carbons. It is important to note that this assumption remains less likely than a cycle opening given the low stability of cycles that contain triple bonds. In addition, the formation of a triple C ≡ N bond could take place at the level of the amino groups (NH_2 and NH) by dehydrogenation with neighboring molecules. This type of reaction is known in organic chemistry and is usually done with an oxidant that catalyzes the reaction. One of the possible synthesis pathways for conversion of amines to nitriles, from alkyl or aryl groups, involves oxidizing photocatalytic systems with the use of blue light (Patil and Gupta, 2020). The hypothesis of a nitrile group is therefore, for the moment, the most consistent with regard to the structure of nucleobases. Although such a compound may have been detected by UHPLC-HRMS, they have not yet been identified. More investigation would require the study of photochemical degradation of uracil and its dimers by computational methods. However, this indicates an increase in the complexity of chemical functions formed by irradiation of uracil in the presence of perchlorates. This band is observed for irradiation times above 120 min. This chemical function has a high probability to form from the first photoproducts formed during the first minutes of irradiation.

Previous studies with the MOMIE setup and low Earth orbit experiments on other organic molecules such as glycine and adenine (Poch *et al.,* 2014; Stalport *et al.,* 2019) have shown that these compounds should not accumulate at the surface of Mars. By comparing the Φ_{exp} of uracil, without calcium perchlorate (0.30 ± 0.26 molecule·photon^{-1}) and with this calcium perchlorate (12.3 ± 8.3 molecule·photon^{-1}), to the Φ_{exp} of these compounds (less than 10^{-3} molecule·photon^{-1}), it appears that uracil is photolyzed much faster than most organic molecules previously studied. Consequently, uracil should not be present in the first centimeters of the surface layer of Mars. However, the formation of photoproduced dimers was observed all along the experiments, with or without calcium perchlorates. Therefore, the search of uracil as an astrobiologically relevant molecule should be oriented toward the search of the uracil dimers.

Finally, IR spectroscopy analyses of our uracil samples irradiated in the presence of calcium perchlorate do not allow us to conclude on the formation of chlorinated compounds. Indeed, the IR bands of the C-Cl bond stretching can only be observed below 900 cm^{-1}. Moreover, our UHPLC-HRMS analyses were not conclusive on the detection of chlorinated compounds. Therefore, we cannot identify uracil as a parent molecule of chlorinated compounds detected on the surface of Mars by the SAM instrument on board the MSL rover.

5. Conclusion and Perspectives

This work aimed to study the degradation of uracil under Mars-like UV radiation conditions in the presence of calcium perchlorate with the MOMIE laboratory setup to estimate the effect of strong oxidants on the preservation of such a molecule. FTIR results show that uracil, when exposed to UV radiation in the presence of calcium perchlorate, is quickly photolyzed and produces new compounds. This was confirmed by the experimental efficiency of photodecomposition ($\Phi_{exp} = 12.3 \pm 8.3$ molecule·photon^{-1}), which was more than 30 times higher than Φ_{exp} of pure UV-exposed uracil (0.16 ± 0.14 molecule·photon^{-1}). This means that the presence of calcium perchlorate enhances the photodissociation of uracil. However, FTIR and UHPLC-HRMS results confirmed that some of the uracil dimers formed by the photolysis of uracil are also formed when calcium perchlorate is present in the samples. These dimers should, therefore, be sought in the soil samples analyzed on Mars by space instruments as the presence of calcium perchlorates does not prevent their formation by photolysis. Their potential detection would imply that uracil is most likely the parent molecule. These dimers could be tested in flight-like laboratory conditions in order to determine the best analytical conditions for their detection on Mars. In addition, new chemical functions (most likely C ≡ C and/or C≡N) were detected by FTIR analyses with the exposed sample containing calcium perchlorate. This implies that the presence of these salts might increase the chemical complexity of the photoproducts formed during the simulation experiments and possibly on Mars. The chemical pathways to the formation of such products should be investigated by theoretical studies in order to identify the possible molecules and intermediate reactive photoproducts to search for by UHPLC-HRMS. Because uracil presented a high photochemical reactivity under UV Mars-like conditions that resulted in the formation of more UV-resistant photoproducts, similar nucleobases should be considered. Future studies will focus on the photolysis of other pyrimidines found in meteorites (such as thymine and cytosine) with and without perchlorates to investigate (i) the photodissociation of such UV reactive molecules under Mars-like conditions and (ii) the effect of powerful oxidizing species such as perchlorates on their degradation.

Acknowledgments

UHPLC-HRMS analyses were performed on the PRAMMICS platform. The authors greatly acknowledge the PRAMMICS platform OSU-EFLUVE UMS 3563.

The authors also acknowledge the DIM ACAV (Domaine d'Intéret Majeur—Astrophysique et Conditions de l'Apparition de la Vie) and the French Space Agency ''Centre National d'Etudes Spatiales'' (CNES) for their funding support.

Finally, the authors would like to thank the three interns who worked on this project: C. Beranger, J. Faria, A. Houerbi for their experimental contribution.

Author Disclosure Statement

No competing financial interests exist.

Supplementary Material

Supplementary Information
Supplementary Table S1

Supplementary Figure S1
Supplementary Figure S2
Supplementary Figure S3
Supplementary Figure S4
Supplementary Figure S5
Supplementary Figure S6
Supplementary Figure S7
Supplementary Figure S8
Supplementary Figure S9

References

Alexander COD, Cody G, De Gregorio B, *et al.* The nature, origin and modification of insoluble organic matter in chondrites, the major source of Earth's C and N. *Geochemistry* 2017;77(2):227–256; doi: 10.1016/j.chemer.2017.01.007.

Anderson SL, Boyd PG, Gładysiak A, *et al.* Nucleobase pairing and photodimerization in a biologically derived metal-organic framework nanoreactor. *Nat Commun* 2019;10(1): 1612; doi: 10.1038/s41467-019-09486-2.

Bera PP, Nuevo M, Materese CK, *et al.* Mechanisms for the formation of thymine under astrophysical conditions and implications for the origin of life. *J Chem Phys* 2016;144(14): 144308; doi: 10.1063/1.4945745.

Callahan MP, Smith KE, Cleaves HJ, *et al.* Carbonaceous meteorites contain a wide range of extraterrestrial nucleobases. *Proc Natl Acad Sci USA* 2011;108(34):13995–13998; doi: 10.1073/pnas.1106493108.

Carrier B, Abbey W, Beegle L, *et al.* Attenuation of ultraviolet radiation in rocks and minerals: implications for Mars science. *J Geophys Res Planets* 2019;124(10):2599–2612; doi: 10.1029/2018JE005758.

Carrier BL. Next steps forward in understanding martian surface and subsurface chemistry. *J Geophys Res Planets* 2017; 122(9):1951–1953; doi: 10.1002/2017JE005409.

Carrier BL, Kounaves SP. The origins of perchlorate in the martian soil. *Geophys Res Lett* 2015;42(10):3739–3745; doi: 10.1002/2015GL064290.

Chen Y, Zhang Y-H, Zhao L-J. ATR-FTIR spectroscopic studies on aqueous $LiClO_4$, $NaClO_4$, and $Mg(ClO_4)_2$ solutions. *Phys Chem Chem Phys* 2004;6:537–542; doi: 10.1039/B311768E.

Clark J, Sutter B, Archer Jr PD, *et al.* A review of Sample Analysis at Mars-Evolved Gas Analysis Laboratory analog work supporting the presence of perchlorates and chlorates in Gale Crater, Mars. *Minerals,* 2021;11(5):475; doi: 10.3390/min11050475.

Cottin H. The PROCESS experiment: An astrochemistry laboratory for solid and gaseous organic samples in low-earth orbit. *Astrobiology* 2012;12(5):412–425; doi: 10.1089/ast.2011.0773.

Dartnell LR, Desorgher L, Ward JM, *et al.* Modelling the surface and subsurface martian radiation environment: Implications for astrobiology. *Geophys Res Lett* 2007;34(2); doi: 10.1029/2006GL027494.

Ehlmann BL, Berger G, Mangold N, *et al.* Geochemical consequences of widespread clay mineral formation in Mars' ancient crust. *Space Sci Rev* 2013;174:329–364; doi: 10.1007/s11214-012-9930-0.

Ehresmann B, Zeitlin C, Hassler DM, *et al.* Charged particle spectra obtained with the Mars Science Laboratory Radiation Assessment Detector (MSL/RAD) on the surface of Mars. *J Geophys Res Planets* 2014;119(3):468–479; doi: 10.1002/2013JE004547.

Eigenbrode JL, Summons RE, Steele A, *et al.* Organic matter preserved in 3-billion-year-old mudstones at Gale Crater, Mars. *Science,* 2018;360(6393):1096–1101; doi: 10.1126/science.aas9185.

Farley KA, Williford KH, Stack KM, *et al.* Mars 2020 mission overview. *Space Sci Rev* 2020;216:142; doi: 10.1007/s11214-020-00762-y.

Florián J, Hrouda V. Scaled quantum mechanical force fields and vibrational spectra of solid state nucleic acid constituents V: thymine and uracil. *Spectrochim Acta A* 1993;49(7):921–938; doi: 10.1016/0584-8539(93)80211-R.

Flynn GJ. The delivery of organic matter from asteroids and comets to the early surface of Mars. In *Worlds in Interaction: Small Bodies and Planets of the Solar System.* (Rickman H, Valtonen MJ, *et al.* eds.) Springer: Dordrecht, The Netherlands, 1996; pp 469–474.

Fornaro T, Brucato JR, Pace E, *et al.* Infrared spectral investigations of UV irradiated nucleobases adsorbed on mineral surfaces. *Icarus* 2013;226:1068–1085; doi: 10.1016/j.icarus.2013.07.024.

Fornaro T, Boosman A, Brucato JR, *et al.* UV irradiation of biomarkers adsorbed on minerals under martian-like conditions: Hints for life detection on Mars. *Icarus* 2018;313:38–60; doi: 10.1016/j.icarus.2018.05.001.

Freissinet C, Glavin D, Mahaffy PR, *et al.* Organic molecules in the Sheepbed Mudstone, Gale Crater, Mars. *J Geophys Res Planets* 2015;120(3):495–514; doi: 10.1002/2014JE004737.

Glavin DP, Freissinet C, Miller KE, *et al.* Evidence for perchlorates and the origin of chlorinated hydrocarbons detected by SAM at the Rocknest aeolian deposit in Gale Crater. *J Geophys Res Planets* 2013;118(10):1955–1973; doi: 10.1002/jgre.20144.

Grotzinger JP, Crisp J, Vasavada AR, *et al.* Mars Science Laboratory mission and science investigation. *Space Sci Rev* 2012;170:5–56; doi: 10.1007/s11214-012-9892-2.

Guan YY, Fray N, Coll P, *et al.* UVolution: Compared photochemistry of prebiotic organic compounds in low Earth orbit and in the laboratory. *Planet Space Sci* 2010;58:1327–1346; doi: 10.1016/j.pss.2010.05.017.

Haberle R, Gómez-Elvira J, de la Torre Juárez M, *et al.* Preliminary interpretation of the REMS pressure data from the first 100 sols of the MSL mission. *J Geophys Res Planets* 2014;119(3):440–453; doi: 10.1002/2013JE004488.

Hecht MH, Kounaves SP, Quinn RC, *et al.* Detection of perchlorate and the soluble chemistry of martian soil at the Phoenix lander site. *Science* 2009;325(5936):64–67; doi: 10.1126/science.1172466.

Jaramillo EA, Royle SH, Claire MW, *et al.* Indigenous organic-oxidized fluid interactions in the Tissint Mars meteorite. *Geophys Res Lett* 2019;46(6):3090–3098; doi: 10.1029/2018GL081335.

Knutsen EW, Villanueva GL, Liuzzi G, *et al.* Comprehensive investigation of Mars methane and organics with ExoMars/NOMAD. *Icarus* 2021;357:114266; doi: 10.1016/j.icarus.2020.114266.

Kopitzky R, Grothe H, Willner H. Chlorine oxide radicals ClO_x ($x = 1$–4) studied by matrix isolation spectroscopy. *Chemistry* 2002;8(24):5601–5621; doi: 10.1002/1521-3765(20021216)8:24<5601::AID-CHEM5601>3.0.CO;2-Z.

Kounaves SP, Carrier BL, O'Neil GD, *et al.* Evidence of martian perchlorate, chlorate, and nitrate in Mars meteorite EETA79001: Implications for oxidants and organics. *Icarus,* 2014a;229:206–213; doi: 10.1016/j.icarus.2013.11.012.

Kounaves SP Chaniotakis NK Chevrier VF *et al.* Identification of the perchlorate parent salts at the Phoenix Mars landing site and possible implications. *Icarus,* 2014b;232:226–231; doi: 10.1016/j.icarus.2014.01.016.

Lewis DL, Estes ED, Hodgson DJ. The infrared spectra of coordinated perchlorates. *Journal of Crystal and Molecular Structure* 1975;5:67–74; doi: 10.1007/BF01202553.

Mahaffy PR, Webster CR, Cabane M, *et al.* The Sample Analysis at Mars investigation and instrument suite. *Space Sci Rev* 2012;170:401–478; doi: 10.1007/s11214-012-9879-z.

Martinez G, Vicente-Retortillo A, Renno N, *et al.* Generation of UV radiation data at Gale Crater by correcting REMS UV measurements from dust deposition and sensor's angular response. In *48th Lunar and Planetary Science Conference.* Lunar and Planetary Institute: Houston, 2017; abstract 1842.

Materese CK, Nuevo M, Bera PP, *et al.* Thymine and other prebiotic molecules produced from the ultraviolet photoirradiation of pyrimidine in simple astrophysical ice analogs. *Astrobiology* 2013;13(10):948–962; doi: 10.1089/ast.2013.1044.

Matthia D, Hassler DM, De Wet W, *et al.* The radiation environment on the surface of Mars—summary of model calculations and comparison to RAD data. *Life Sci Space Res (Amst)* 2017;14:18–28; doi: 10.1016/j.lssr.2017.06.003.

McKenna-Lawlor S, Gonçalves P, Keating A, *et al.* Characterization of the particle radiation environment at three potential landing sites on Mars using ESA's MEREM models. *Icarus* 2012;218:723–734; doi: 10.1016/j.icarus.2011.04.004.

Millan M, Teinturier S, Malespin C, *et al.* Organic molecules revealed in Mars's Bagnold Dunes by Curiosity's derivatization experiment. *Nat Astron* 2021;6:129–140; doi: 10.1038/s41550-021-01507-9.

Mustard JF, Murchie S, Pelkey S, *et al.* Hydrated silicate minerals on Mars observed by the Mars Reconnaissance Orbiter CRISM instrument. *Nature*. 2008;454(7202):305–309; doi: 10.1038/nature07097.

Navarro-González R, Vargas E, de la Rosa J, *et al.* Reanalysis of the Viking results suggests perchlorate and organics at midlatitudes on Mars. *J Geophys Res Planets,* 2010; 115(E12); doi: 10.1029/2010JE003599.

Oba Y, Takano Y, Furukawa Y, *et al.* Identifying the wide diversity of extraterrestrial purine and pyrimidine nucleobases in carbonaceous meteorites. *Nat Commun* 2022;13(1): 2008; doi: 10.1038/s41467-022-29612-x.

Patel M, Zarnecki J, Catling D. Ultraviolet radiation on the surface of Mars and the Beagle 2 UV sensor. *Planet Space Sci* 2002;50(9):915–927; doi: 10.1016/S0032-0633(02)00067-3.

Patil RD, Gupta MK. Methods of nitriles synthesis from amines through oxidative dehydrogenation. *Adv Synth Catal* 2020; 362(19):3987–4009; doi: 10.1002/adsc.202000635.

Pizzarello S, Cooper G, Flynn G. The nature and distribution of the organic material in carbonaceous chondrites and interplanetary dust particles. In *Meteorites and the Early Solar System II.* (Lauretta DS, McSween HY. eds.) University of Arizona Press: Tucson, 2006; pp 625–651.

Poch O, Noblet A, Stalport F, *et al.* Chemical evolution of organic molecules under Mars-like UV radiation conditions simulated in the laboratory with the ''Mars Organic Molecule Irradiation and Evolution'' (MOMIE) setup. *Planet Space Sci* 2013;85:188–197; doi: 10.1016/j.pss.2013.06.013.

Poch O, Kaci S, Stalport F, *et al.* Laboratory insights into the chemical and kinetic evolution of several organic molecules under simulated Mars surface UV radiation conditions. *Icarus*. 2014;242:50–63; doi: 10.1016/j.icarus.2014.07.014.

Poulet F, Bibring J-P, Mustard J. F, *et al.* Phyllosilicates on Mars and implications for early martian climate. *Nature* 2005;438(7068):623–627; doi: 10.1038/nature04274.

Rouquette L, Stalport F, Cottin H, *et al.* Dimerization of uracil in a simulated Mars-like UV radiation environment. *Astrobiology,* 2020;20(11):1363–1376; doi: 10.1089/ast.2019.2157.

Saïagh K, Cottin H, Aleian A, *et al.* VUV and mid-UV photoabsorption cross sections of thin films of guanine and uracil: application on their photochemistry in the Solar System. *Astrobiology,* 2015;15(4):268–282; doi: 10.1089/ast.2014.1196.

Schmitt-Kopplin P, Gabelica Z, Gougeon RD, *et al.* High molecular diversity of extraterrestrial organic matter in Murchison meteorite revealed 40 years after its fall. *Proc Natl Acad Sci USA* 2010;107(7):2763–2768; doi: 10.1073/pnas.0912157107.

Schuttlefield JD, Sambur JB, Gelwicks M, *et al.* Photooxidation of chloride by oxide minerals: Implications for perchlorate on Mars. *J Am Chem Soc* 2011;133:17521–17523; doi: 10.1021/ja2064878.

Sephton MA. Organic compounds in carbonaceous meteorites. *Nat Prod Rep* 2002;19:292–311; doi: 10.1039/B103775G.

Stalport F, Rouquette L, Poch O, *et al.* The Photochemistry on Space Station (PSS) experiment: Organic matter under Mars-like surface UV radiation conditions in low Earth orbit. *Astrobiology,* 2019;19(8):1037–1052; doi: 10.1089/ast.2018.2001.

Susi H, Ard JS. Vibrational spectra of nucleic acid constituents—I: Planar vibrations of uracil. *Spectrochim Acta A* 1971; 27(9)1549–1562; doi: 10.1016/0584-8539(71)80211-8.

Svensson T, Nelander B, Bernhardsson A, *et al.* Infrared spectroscopic and *ab initio* study of $HOOClO_2$. *J. Phys Chem A* 1999;103(23):4432–4437; doi: 10.1021/jp990070w.

Szopa C, Freissinet C, Glavin DP, *et al.* First detections of dichlorobenzene isomers and trichloromethylpropane from organic matter indigenous to Mars mudstone in Gale Crater, Mars: Results from the Sample Analysis at Mars instrument onboard the Curiosity rover. *Astrobiology* 2020;20(2):292–306; doi: 10.1089/ast.2018.1908.

ten Kate IL, Garry JR, Peeters Z, *et al.* The effects of martian near surface conditions on the photochemistry of amino acids. *Planet Space Sci* 2006;54(3):296–302; doi: 10.1016/j.pss.2005.12.002.

Vago JL, Westall F, Coates AJ, *et al.* Habitability on early Mars and the search for biosignatures with the ExoMars Rover. *Astrobiology* 2017;17(6–7):471–510; doi: 10.1089/ast.2016.1533.

Vicente-Retortillo A, Martínez GM, Rennó NO, *et al. In Situ* UV Measurements by MSL/REMS: Dust deposition and angular response corrections. *Space Sci Rev* 2020;216:97; doi: 10.1007/s11214-020-00722-6.

Wu Z, Wang A, Farrell WM, *et al.* Forming perchlorates on Mars through plasma chemistry during dust events. *Earth Planet Sci Lett* 2018;504:94–105; doi: 10.1016/j.epsl.2018.08.040.

Zhang X, Berkinsky D, Markus CR, *et al.* Reaction of methane and UV-activated perchlorate: Relevance to heterogeneous

loss of methane in the atmosphere of Mars. *Icarus,* 2022;376: 114832; doi: 10.1016/j.icarus.2021.114832.

Address correspondence to:
F. Stalport
LISA - UPEC - Faculté des Sciences et Technologie
61 avenue général de Gaulle
Créteil Cédex 94010
France

E-mail: fabien.stalport@gmail.com

Submitted 11 December 2022
Accepted 2 July 2023
Associate Editor: Christopher McKay

Abbreviations Used

CCS = Cross Collision Section
FTIR = Fourier transformation infrared
MOMIE = Mars Organic Matter Irradiation and Evolution
MSL = Mars Science Laboratory
REMS = Rover Environmental Monitoring Station
SAM = Sample Analysis at Mars
UHPLC-HRMS = ultra-high-performance liquid chromatography coupled with high-resolution mass spectrometry
UVS = UV sensor